



1

2 **Growing-season variability and environmental controls of CH<sub>4</sub> and**  
3 **N<sub>2</sub>O fluxes across high-latitude terrestrial ecosystems**

4

5 Johannes Niemi<sup>1,2</sup>, Miska Luoto<sup>1</sup>, Anna-Maria Virkkala<sup>1,3,4</sup>, Johanna Lehtinen<sup>1</sup>, Jenni  
6 Hultman<sup>2</sup>

7 <sup>1</sup> Department of Geosciences and Geography, University of Helsinki, Finland; johannes.niemi@helsinki.fi

8 <sup>2</sup> Soil ecosystems, Luke (Natural resources institute), Finland

9 <sup>3</sup> Climate research unit, FMI (Finnish Meteorological institute), Finland

10 <sup>4</sup> Woodwell Climate Research Center, USA

11

12 Correspondence: Johannes Niemi, johannes.niemi@helsinki.fi

13

14 ORCID:

15 Johannes Niemi [0009-0002-1042-3173](https://orcid.org/0009-0002-1042-3173)

16 Miska Luoto [0000-0001-6203-5143](https://orcid.org/0000-0001-6203-5143)

17 Anna-Maria Virkkala [0000-0003-4877-2918](https://orcid.org/0000-0003-4877-2918)

18 Johanna Lehtinen [0009-0001-2350-141X](https://orcid.org/0009-0001-2350-141X)

19 Jenni Hultman [0000-0002-3431-1785](https://orcid.org/0000-0002-3431-1785)



## 20 **Abstract**

21 Rapid warming and accelerating ecological change across high-latitude (>66°N) terrestrial  
22 environments are reshaping greenhouse gas dynamics. However, spatiotemporal patterns and  
23 environmental drivers of CH<sub>4</sub> and N<sub>2</sub>O fluxes in high-latitude ecosystems remain poorly  
24 understood.

25 In this study we describe the seasonal and spatial variation in CH<sub>4</sub> and N<sub>2</sub>O fluxes  
26 across key subarctic and boreal environmental gradients. A secondary aim is to examine the  
27 environmental drivers underlying these flux patterns. We measured fluxes during the snow-  
28 free season of 2024 and 2025 in northern Finland, starting early June (spring snowmelt) and  
29 ending late September (first snowfall). We conducted 1272 chamber measurements at 144  
30 locations spanning eight high-latitude land cover classes: bare tundra, dwarf-shrub tundra,  
31 deciduous forest, evergreen forest, fen, bog, permafrost bog and tundra wetland.

32 Forest and dry tundra sites acted as net CH<sub>4</sub> sinks (-0.16 to -0.05 mg m<sup>-2</sup> h<sup>-1</sup>,  
33 depending on land cover class) and as both N<sub>2</sub>O sources and sinks (-0.69 to 1.69 μg m<sup>-2</sup> h<sup>-1</sup>).  
34 Wetlands were net CH<sub>4</sub> sources (0.93 to 27.81 mg m<sup>-2</sup> h<sup>-1</sup>) and net N<sub>2</sub>O sinks (-0.89 to -6.53  
35 μg m<sup>-2</sup> h<sup>-1</sup>). Highest mean CH<sub>4</sub> fluxes occurred in fens (23.4 mg m<sup>-2</sup> h<sup>-1</sup>) and permafrost bogs  
36 (27.8 mg m<sup>-2</sup> h<sup>-1</sup>) which often coincided with substantial N<sub>2</sub>O sinks (-4.68 μg m<sup>-2</sup> h<sup>-1</sup>).  
37 Seasonal trends were present for CH<sub>4</sub> but were land cover-dependent, with both sinks and  
38 sources typically peaking during July–August. Land cover class, soil temperature, and soil  
39 pH had the strongest effects on CH<sub>4</sub> fluxes while variation in N<sub>2</sub>O was best explained by soil  
40 pH and land cover class. However, a significant portion of the variability in N<sub>2</sub>O remained  
41 unexplained.

42 These results demonstrate that strong spatial heterogeneity and pronounced seasonal  
43 dynamics during the snow-free period generate substantial variability in CH<sub>4</sub> and N<sub>2</sub>O fluxes  
44 across high-latitude ecosystems. Our findings suggest that monthly measurements of *in-situ*  
45 gas fluxes and soil conditions in combination with accurate land cover mapping are essential  
46 for modelling and upscaling of GHG fluxes. This is especially important in high-latitude  
47 regions, where rapid warming is altering both ecosystem distributions and soil conditions  
48 with significant consequences for current and future GHG budgets.

49

50



## 51           **1. Introduction**

52           High-latitude (>66°N) ecosystems exhibit highly dynamic greenhouse gas (GHG) fluxes  
53           shaped by the interactions of soil, microbial, and vegetation processes (Whalen et al., 2005;  
54           Riutta et al., 2007; Olefeldt et al., 2013; Martins et al., 2017). Climate change can alter all  
55           these factors by reshaping abiotic conditions such as precipitation, temperature, and snow  
56           cover. Changing climate also drives biological shifts, including changes in microbial  
57           communities (Deslippe et al., 2012) and broader ecosystem transitions such as shrubification,  
58           paludification, and permafrost thaw (Myers-Smith et al., 2011; Biskabjorn et al., 2019).  
59           Arctic regions store a major fraction of global soil carbon reserves (Batjes et al., 2016;  
60           Hugelius et al., 2020) and are warming faster than the global average (Rantanen et al., 2022),  
61           underscoring their importance in the global carbon cycle. However, the interplay of complex  
62           GHG processes and the heterogeneous landscape makes both measurements and modelling  
63           particularly challenging.

64                        Soil carbon storage and GHG dynamics vary widely across high-latitude ecosystems  
65                        (Hugelius et al., 2024). Peatlands, for example, function as major long-term carbon sinks due  
66                        to ongoing peat accumulation, yet they are also the largest natural source of atmospheric  
67                        methane (CH<sub>4</sub>) because of their persistently anoxic soils (Saunois et al., 2025; Kübert et al.,  
68                        2026). Although tundra and forest ecosystems store less carbon per unit area than peatlands,  
69                        their vast extent means they exert a major influence on high-latitude carbon cycling through  
70                        CH<sub>4</sub> uptake, biomass and soil carbon storage, and GPP (Virkkala et al., 2021; Li et al 2025;  
71                        Jiang et al., 2025). In addition to CH<sub>4</sub> dynamics, nitrous oxide (N<sub>2</sub>O) sources and sinks have  
72                        been reported from high-latitude ecosystems, but their magnitudes, spatial patterns, and  
73                        environmental drivers remain poorly understood (Chapuis-Lardy et al., 2007; Maruschak et  
74                        al., 2011; Voigt et al., 2020). N<sub>2</sub>O has a global warming potential roughly 280–300 times that  
75                        of CO<sub>2</sub> and is the third most influential greenhouse gas after CO<sub>2</sub> and CH<sub>4</sub> (IPCC, 2014).

76                        Wetlands have a disproportionately strong effect on carbon dynamics due to their  
77                        intense CH<sub>4</sub> emissions and large soil carbon stocks and because of that, they are  
78                        overrepresented in many flux databases (Kuhn et al., 2021; Virkkala et al., 2025, preprint).  
79                        Yet, high-latitude landscapes are heterogenous with a mosaic composition of wetlands,  
80                        forests and tundra of which dry tundra soils are especially underrepresented in literature.  
81                        Furthermore, it is typical to focus on peak growing season fluxes (Olefeldt 2013, Kuhn et al.,  
82                        2021) as it makes measurements and modelling more straightforward. However, this ignores



83 the strong seasonal dynamics of the environmental drivers in high-latitude ecosystems which  
84 control GHG fluxes (Rautakoski et al., 2024; Kübert et al., 2026). Multi-month  
85 measurements across ecosystems are therefore required to resolve the seasonal progression of  
86 GHG fluxes and their underlying controls, which can shift substantially across environmental  
87 gradients and between spring, summer peak productivity, and autumn transition.

88 This study aims to characterize the seasonal and spatial variability of CH<sub>4</sub> and N<sub>2</sub>O  
89 fluxes across key subarctic and boreal land cover classes, focusing on representative forest,  
90 wetland, and tundra ecosystems. A secondary aim is to examine the key environmental  
91 drivers and their role in shaping these flux patterns. To capture ecosystem-level  
92 heterogeneity, we classify these biomes into eight land cover classes following the BAWLD  
93 dataset framework (Olefeldt et al., 2021, Kuhn et al., 2021): deciduous and evergreen forests,  
94 bare tundra, dwarf-shrub tundra, fens, bogs, permafrost bogs and tundra wetlands.  
95 Specifically, we address three research questions: (i) How do CH<sub>4</sub> and N<sub>2</sub>O fluxes differ  
96 among the land cover classes? (ii) How do these fluxes develop seasonally during the snow-  
97 free period (June–September)? (iii) How do various environmental variables explain the  
98 variance in GHG fluxes? The analysis is based on 1273 *in situ* chamber measurements  
99 collected at 144 locations spanning eight high-latitude land cover classes. The measurements  
100 cover the full duration of growing seasons of years 2024 and 2025, from spring snowmelt to  
101 late autumn.

102



103

## 2. Materials & methods



104

105 **Figure 1.** Research sites and land cover classifications (Photos: Niemi J., Mäki-Ikola S.).  
106 The research plots are divided between two locations, subarctic Kilpisjärvi (top left) and  
107 boreal Pallas (top right) which are further categorized into eight different land cover  
108 classes. Red dots on the maps are the locations of the measurement plots (n=144).



## 109 **2.1 Location and area descriptions**

110 The two study locations are in the Pallas-Yllästunturi national park in the Kittilä and Muonio  
111 municipalities in western Finnish Lapland, and the Kilpisjärvi region in the Enontekiö  
112 municipality, in northwestern Finnish Lapland. The Pallas study sites (67.9° N, 24.0° E, 250–  
113 570 m a.s.l) are located at the edge of the northern-boreal and subarctic climatic zones with a  
114 long-term mean annual temperature of  $-1.0$  °C and annual precipitation of 644 mm (Pirinen  
115 et al., 2012). It is characterized by a mosaic of northern boreal ecosystems consisting of  
116 mixed and coniferous forests (*Picea abies*, *Pinus sylvestris*, *Betula pubescens*), open fen  
117 wetlands and open tundra on the fells. The Kilpisjärvi (Gilbbesjávri in Northern Sámi  
118 language) study sites are located in the subarctic climate zone (69.0° N, 20.8° E, 474–737 m  
119 a.s.l) with a long-term mean annual temperature of  $-1.9$  °C and annual precipitation of  
120 487 mm (Pirinen et al., 2012). The Kilpisjärvi region lies at the ecotone between the boreal  
121 and tundra biomes and is characterized by dwarf-shrub dominated tundra highlands, *Carex*  
122 spp. dominated open fens and short stature mountain birch (*Betula pubescens* var *pumila*)  
123 forests at lower altitudes. In addition, some of the wetlands in the region are palsa mires,  
124 characterized by permanently frozen peat hummocks which are rapidly degrading under  
125 current climate conditions. Soil conditions differed markedly between Pallas and Kilpisjärvi.  
126 The Pallas area is underlain by acidic Precambrian bedrock, resulting in low soil pH, whereas  
127 Kilpisjärvi is characterized by a geological mosaic of Paleozoic sedimentary rocks and acidic  
128 Precambrian bedrock (Simonen, 1990), yielding intermediate soil pH conditions. This  
129 geological contrast provides a robust framework for assessing the influence of soil properties  
130 on CH<sub>4</sub> and N<sub>2</sub>O fluxes. Snowmelt and associated flooding and nutrient pulses typically  
131 occur in June, with rapidly increasing daylight hours progressing into a ~2-month period of  
132 continuous daylight from late-May to late-July. Afterwards, a senescing period with  
133 occasional sub-zero temperatures occurs already during September. All measurement areas  
134 are relatively undisturbed with no ditching, recent logging or other major human influences.

## 135 **2.2 Field campaign**

136 The measurement campaign was conducted in two parts (years 2024 and 2025). The first part  
137 took place between 9th of June and 1st of October (2024) and the second part between 3rd of  
138 June and 21st of September (2025). A total of 144 measurement plots were repeatedly  
139 sampled once a month (Jun–Jul–Aug–Sept.) each year. Additional repeated measurements  
140 were taken from roughly a third of the research plots. In total, we conducted 1273 chamber



141 measurements (n=1273 for each GHG) while continuously measuring microclimate and green  
142 vegetation cover at each measurement plot.

### 143 **2.3 Land cover classification and vegetation**

144 The measurement plots were equally distributed between the Pallas (boreal) and Kilpisjärvi  
145 (subarctic) regions and further divided between eight different key land covers: bare tundra,  
146 shrubby tundra, evergreen forest, deciduous forest, tundra wetland, bog, fen and permafrost  
147 bog (palsas). These land cover categorizations are based on the BAWLD-CH<sub>4</sub> dataset (Kuhn  
148 et al., 2021, Olefeldt et al., 2021), with some minor changes to more accurately describe our  
149 research sites. Specifically, our tundra wetland sites are not permafrost affected, and we  
150 separated dry upland soils into bare tundra and shrubby tundra as we expected them to have  
151 very different GHG flux profiles due to differences in vegetation cover and organic layer  
152 thickness.

153 Shrub tundra plots (n=28) are located above the tree line and typically have a thin dry organic  
154 soil layer with low nutrient availability. Vegetation is generally dominated by *Betula nana*,  
155 *Empetrum nigrum* and *Vaccinium myrtillus*, although vegetation can occasionally be more  
156 diverse in wind protected valleys and creeks. Bare tundra plots (n=11) lack vascular plants  
157 and typically result from repeating freeze-melt cycles (cryoturbation) and persistent winds at  
158 higher altitudes. These plots may occasionally support small amounts of lichen and mosses.

159 Evergreen forest plots (n=21) are located at the northern edge of the boreal zone have a tree  
160 cover dominated by *Picea abies* or *Pinus sylvestris* but can also have some deciduous trees  
161 mixed in, i.e. *Betula pubescens* or *Populus tremula*. Field layer is dominated by dwarf-shrubs  
162 (e.g. *V. myrt.*, *V. vitis-idaea*) and various graminoids (e.g. *Avenella* spp. and *Poa* spp.) The  
163 deciduous forest plots (n=20) are primarily located below the forest limit, and the tree cover  
164 consists solely of short growing *Betula pubescens* var. *pumila* (mountain birch). The field  
165 layer is mixed with various dwarf-shrubs, graminoids (*Avenella* spp.) and forbs (e.g. *Cornus*  
166 *suecica*, *Viola palustris*).

167 Fen plots (n=31) are minerotrophic, wet and treeless wetlands with peat depths up to ~4 m.  
168 Field layer is dominated by *Carex* spp. and *Sphagnum* spp. Bog plots (n=11) are all of the dry  
169 and “hummocky” (permafrost free) wetland forms, i.e. if a wetland as a whole would be  
170 considered a fen, it might still have elevated dry *Sphagnum* hummocks with bog-type  
171 shrubby vegetation which have considerably different greenhouse gas profiles compared to  
172 the wetter fen-type areas. Permafrost bog plots (palsa mires, n=10) are similar to the



173 previously mentioned bogs but with permafrost cores that are in various stages of  
174 degradation. The permafrost bog research sites include two different peatlands representing  
175 varying degrees of permafrost degradation: one with largely intact but degrading palsas, the  
176 other with only remnants of old permafrost left. Lastly, tundra wetland plots (n=12) are  
177 *Carex* spp., *Trichoforum* spp. and moss dominated wetlands (note: generally, no *Sphagnum*  
178 spp.). They have shallow organic soil layers (with little to no peat accumulation) underlined  
179 with fluvial deposits and mineral soil with variable seasonal hydrology, i.e. wet during spring  
180 snowmelt but can be very dry during summer. These are typically situated on hillsides with  
181 small creeks running through them.

#### 182 **2.4. Environmental variables**

183 The field layer vegetation cover of each plot was estimated by image analysis with Canopeo  
184 (Patriгани and Ochsner 2015). Canopeo measures the relative number of green pixels from a  
185 photo and converts them into percentages, i.e. it acts as a measurement for green vegetation  
186 cover (“vegetation cover”). A photo was taken of each measurement plot every time chamber  
187 measurements were conducted. The pictures covered roughly a 1 m<sup>2</sup> square around the  
188 measurement plot and thus included vegetation from outside the chamber collar.

189 Microclimatic variables were measured with TOMST TMS-4 sensors (Wild et al.,  
190 2019), which are located 0.5–1 m from the chamber collar and measure continuously  
191 throughout the year. Loggers record microclimatic variables in 15-minute intervals: soil  
192 temperature at a depth of -6 cm and soil moisture at depth of -14 cm. Each logger operated  
193 with a temperature resolution of 0.0625 °C and an accuracy of ±0.5 °C. For the soil  
194 temperature, the data quality control and processing procedures followed the approach  
195 outlined in Aalto et al., (2022). First the temperature time series were visually inspected to  
196 remove readings that clearly reflected sensor malfunction, such as abrupt shifts in soil  
197 moisture or temperature indicative of the logger being displaced. After the first screening of  
198 the data, the temperature sensors were then calibrated based on their individual response  
199 differences when stored under stable conditions (i.e. data logged while in storage indoors).  
200 Finally, any abnormal spikes in the data were filtered out, for example, a data point was  
201 flagged as erroneous if soil temperature change between consecutive time steps exceeded 5  
202 °C or change in air temperature exceeded 10 °C.

203 For the soil moisture data, the quality control and preprocessing of the data followed  
204 the same outline as in Kemppinen et al., (2023). Similarly to the temperature time series, the



205 raw soil moisture data was screened manually for clearly erroneous data where values were  
206 removed if the logger had been displaced, or the raw soil moisture value was  $<200$ , as it is  
207 outside the range of the sensor and usually indicates of poorly placed logger. The TOMST  
208 logger records raw soil moisture data based on electromagnetic pulses, producing time-  
209 domain transmission measurements (see Wild et al., 2019 for details). These were  
210 subsequently converted to volumetric water content (VWC, %) using the generic calibration  
211 function for unknown soils by Kopecký et al., (2021). The function for unknown soils was  
212 chosen, as it provided more realistic ranges of VWC values compared to soil-specific  
213 calibrations, however it does limit the maximum possible VWC to 60%. This method has  
214 already been validated in Finland by Kemppinen et al., (2023), supporting its applicability to  
215 this research. After quality control and preprocessing, microclimate data was coupled with  
216 flux measurements by selecting the nearest 15-minute logger reading corresponding to the  
217 flux measurement time. In cases where the closest time point contained erroneous or missing  
218 data, the next closest valid reading was used.

219 Both water table depth and soil moisture have been identified as key drivers for GHG  
220 fluxes (Moore and Dalva 1993; Olefeldt et al., 2013; Rinne et al., 2018; Voigt et al 2020;  
221 Virkkala et al., 2024). We chose to use soil moisture over water table depth for three reasons:  
222 a) determining water table depth in mineral soils typically requires invasive methods that  
223 disturb soil structure and alter hydrological conditions b) water table in tundra and forest sites  
224 is generally very deep, thus it has minimal impact on biogeochemistry occurring at the  
225 surface or at intermediate depths c) we wanted model parameters that can be measured at all  
226 sites (i.e. both mineral soils and wetlands) for robust modelling across ecosystem gradients.

227 Soil samples for pH data were collected once during the measurement campaign from  
228 the organic layer underneath the vegetation (outside the chamber collars). The laboratory  
229 analysis was conducted by the Finnish Natural Resources Institute (LUKE) according to the  
230 ISO 10390 soil Quality-Determination of pH standards.

## 231 **2.5 Chamber measurements and flux calculations**

232 The gas measurements were conducted as closed opaque chamber measurements with a  
233 duration of 3 minutes, taken with two portable gas analyzers (LI-COR-LI7810 and LI-COR-  
234 LI7820) that measure gas concentrations in 1 second intervals. Gas fluxes for  $\text{CH}_4$  and  $\text{N}_2\text{O}$   
235 were both measured simultaneously from the same chamber.



236 The chamber had a built-in fan and a wireless Bluetooth temperature sensor (Ruuvi  
237 tag pro) for measuring chamber temperatures. The volume of the chamber was ~7.85 liters  
238 (cylindrical, 20 x 25 cm) and was placed on top of a steel collar. As the collar height changed  
239 between measuring plots (depending on how soft and deep the soil was), the height was  
240 always measured separately for each gas measurement to get accurate chamber volumes. For  
241 wetlands, the collars were installed into the soil roughly 7–14 days before the measurement  
242 campaign started to avoid disturbances in the peat that could cause ebullition or other  
243 artefacts in the flux. For mineral soils, the collar was removed between measurements to  
244 minimize changes in microclimatic conditions such as sheltering from wind. If unusually  
245 high fluxes were measured, they were repeated multiple times *in situ* to make sure the  
246 emissions were not caused by any influence of the measurer (i.e. ebullition due to the  
247 pressure on surrounding soil). If the repeat measurement showed similar fluxes, then the  
248 initial measurement was used (assuming linear change of gas concentration).

249 Fluxes were calculated as shown in Eq. (1), based on a linear fit between starting gas  
250 concentration at the start of the measurement and at the end of the measurement, utilizing the  
251 ideal gas law

(1)

$$flux = \frac{(ct - c0) \cdot V \cdot M \cdot p}{t \cdot R \cdot (T + 273.15) \cdot A}$$

254 where  $(ct - c0) / t$  is the slope (expressed as ppm s<sup>-1</sup>),  $V$  is chamber volume,  $M$  is molar mass,  
255  $p$  is atmospheric pressure,  $R$  is the ideal gas constant,  $T$  is chamber temperature and  $A$  is  
256 chamber area. Fluxes were also converted from s<sup>-1</sup> to h<sup>-1</sup> and from grams to micrograms and  
257 milligrams. Final units used for fluxes are mg m<sup>-2</sup> h<sup>-1</sup> for CH<sub>4</sub> and µg m<sup>-2</sup> h<sup>-1</sup> for N<sub>2</sub>O.

258 Each chamber measurement was visually graphed to make sure the gas concentrations were  
259 changing linearly and to remove any possible measurement errors, such as anomalies at the  
260 start and end of the measurements that come from pressure changes or from handling the  
261 chamber (Pavelka et al., 2018). The same flux calculation method has been used in previous  
262 studies by Rissanen et al., (2023), Karjalainen et al., (2025) and Suominen et al., (2026).

263 Python script for flux calculations is also available: [https://github.com/janivaltteri/manual-](https://github.com/janivaltteri/manual-chamber-dataserver/blob/main/dataserver/application/fluxcalc.py)  
264 [chamber-dataserver/blob/main/dataserver/application/fluxcalc.py](https://github.com/janivaltteri/manual-chamber-dataserver/blob/main/dataserver/application/fluxcalc.py)



265 Clear measurement errors (i.e. flat zero measurements that are sometimes caused by LI-COR  
266 malfunction) were removed, but all other measurements which had linear gas concentration  
267 change were kept in the data. Non-linear fluxes are typically caused by the increasing  
268 concentration gradient at high gas concentrations, which slows down the gas diffusion rates  
269 from the soil to the chamber causing a log-curve (Pihlatie et al., 2013). In such cases, only the  
270 linear part of the measurement was used for the calculation to avoid underestimating fluxes.  
271 Chamber measurements that showed exponential concentration growth were typically  
272 repeated *in situ* until a linear trend was observed, as this kind of flux behavior is usually  
273 caused by influence of the measurer (Pavelka et al., 2018).

## 274 **2.6 Statistical analysis and modelling**

275 We used the *lme4* package (Bates, Maechler & Bolker 2012) in R (R Core Team,  
276 2024) to fit linear mixed-effects models examining the relationships between GHG fluxes and  
277 environmental variables. We used a joint model for both wetlands and non-wetland soils to  
278 investigate useful parameters for modelling across broad environmental gradients. The final  
279 model for CH<sub>4</sub> consisted of four fixed effects, three two-way interactions terms and a random  
280 effect. As the main effects, we included soil temperature (continuous), soil moisture  
281 (continuous), pH (continuous) and land cover (categorical, 8 levels). Interaction terms were  
282 land cover paired with each of the other fixed variables. The land cover interaction term was  
283 used to give the model flexibility for the direction of the GHG flux response, e.g. increasing  
284 temperature can have both positive and a negative effect on GHG flux depending on the land  
285 cover class. Measurement point identification was used as a random effect (random intercept)  
286 to account for the repeated measurements design (e.g. pseudoreplication). Green vegetation  
287 cover (continuous) and measurement year (categorical, 2 levels) were also tested as fixed  
288 effects but were dropped due to worse model performance.

289 The final model for N<sub>2</sub>O consisted of five fixed effects, two two-way interactions and  
290 a random effect. As main effects we included soil temperature (continuous), pH (continuous),  
291 Green vegetation cover (continuous), year (categorical, 2 levels) and land cover (categorical,  
292 8 levels). Interaction terms were land cover paired with pH and vegetation cover.  
293 Measurement point identification was used as a random effect (random intercept). Soil  
294 moisture, soil moisture-land cover interaction and soil temperature-land cover interaction  
295 were also tested as fixed effects but were dropped due to worse model performance.



296 Model validation was done through Akaike information criterion (AIC) and model  
297 parameter effects sizes were described with partial eta-squared ( $\eta^2p$ ). The GHG flux data was  
298 skewed and included both negative and positive values and as such was normalized with a  
299 YeoJohnson-transformation (Yeo and Johnson, 2000) for CH<sub>4</sub> and with arcsinh-  
300 transformation for N<sub>2</sub>O. Optimal data transformation options were investigated with the  
301 *bestNormalize* R-package (Peterson, 2021). Statistical differences between months were  
302 tested with Aligned Rank Transformed Anova, (ART-Anova, Wobbrock et al., 2011) using  
303 the *ARTool* R-package (Kay et al., 2025). This allows testing for differences between groups  
304 (months) while accounting for repeated measurements and uneven group sizes. Post-Hoc tests  
305 were done following the ART-C contrast testing procedure (Elkin et al., 2021) with Tukey's  
306 HSD using the *art-contrasts* R-package (Elkin et al., 2021).

### 307 **3. Results**

#### 308 **3.10 CH<sub>4</sub> between land cover classes**

309 All dry land cover classes (shrub and bare tundra, deciduous and evergreen forest) were small  
310 net sinks (mean  $-0.12 \text{ mg m}^{-2} \text{ h}^{-1}$ ) for CH<sub>4</sub> and conversely all wetland classes were net  
311 sources (mean  $17.1 \text{ mg m}^{-2} \text{ h}^{-1}$ ) of CH<sub>4</sub> (Fig. 2a), fluxes across all measurements varied from  
312  $-0.55$  to  $1008 \text{ mg m}^{-2} \text{ h}^{-1}$  (Table A1). Highest positive mean CH<sub>4</sub> fluxes were measured from  
313 permafrost bogs (mean  $27.8 \text{ mg m}^{-2} \text{ h}^{-1}$ ; range  $-0.24$  to  $602$ ), followed by fens ( $23.4 \text{ mg m}^{-2}$   
314  $\text{h}^{-1}$ ;  $0.13$  to  $1008$ ), bogs ( $10.1 \text{ mg m}^{-2} \text{ h}^{-1}$ ;  $-0.11$  to  $668$ ) and tundra wetlands ( $0.93 \text{ mg m}^{-2} \text{ h}^{-1}$ ;  
315  $-0.04$  to  $7.59$ ). Largest negative mean CH<sub>4</sub> fluxes (sinks) were measured from shrub tundra  
316 ( $-0.16 \text{ mg m}^{-2} \text{ h}^{-1}$ ;  $-0.55$  to  $0.001$ ) followed by bare tundra ( $-0.13 \text{ mg m}^{-2} \text{ h}^{-1}$ ;  $-0.52$  to  $0.01$ ),  
317 deciduous forests ( $-0.12 \text{ mg m}^{-2} \text{ h}^{-1}$ ;  $-0.50$  to  $3.02$ ) and lastly evergreen forests ( $-0.045 \text{ mg m}^{-2}$   
318  $\text{h}^{-1}$ ;  $-0.40$  to  $0.57$ ). Although both deciduous and evergreen forest were net sinks, they also  
319 included some small positive fluxes which all came from locations in ecotones adjacent to  
320 wetlands or streams.

#### 321 **3.11 CH<sub>4</sub> temporal trends**

322 Across all land cover types, both negative and positive fluxes were small in early June,  
323 increased to their highest values during July–August, and declined again in September.  
324 However, the magnitude of monthly differences was dependent on land cover type (Table  
325 A5). Wetland sites remained net sources throughout the measurement period, with positive  
326 fluxes persisting until the end of the growing season. (Fig. 2a). Within-plot variability across



327 months was often high, but extreme values typically originated from the same few  
 328 measurement locations. For example, one permafrost bog plot, across multiple months,  
 329 produced repeated CH<sub>4</sub> outliers of 50, 116, 366, and 602 mg m<sup>-2</sup> h<sup>-1</sup>, resulting in a within-plot  
 330 range of over 500 mg m<sup>-2</sup> h<sup>-1</sup>.

331

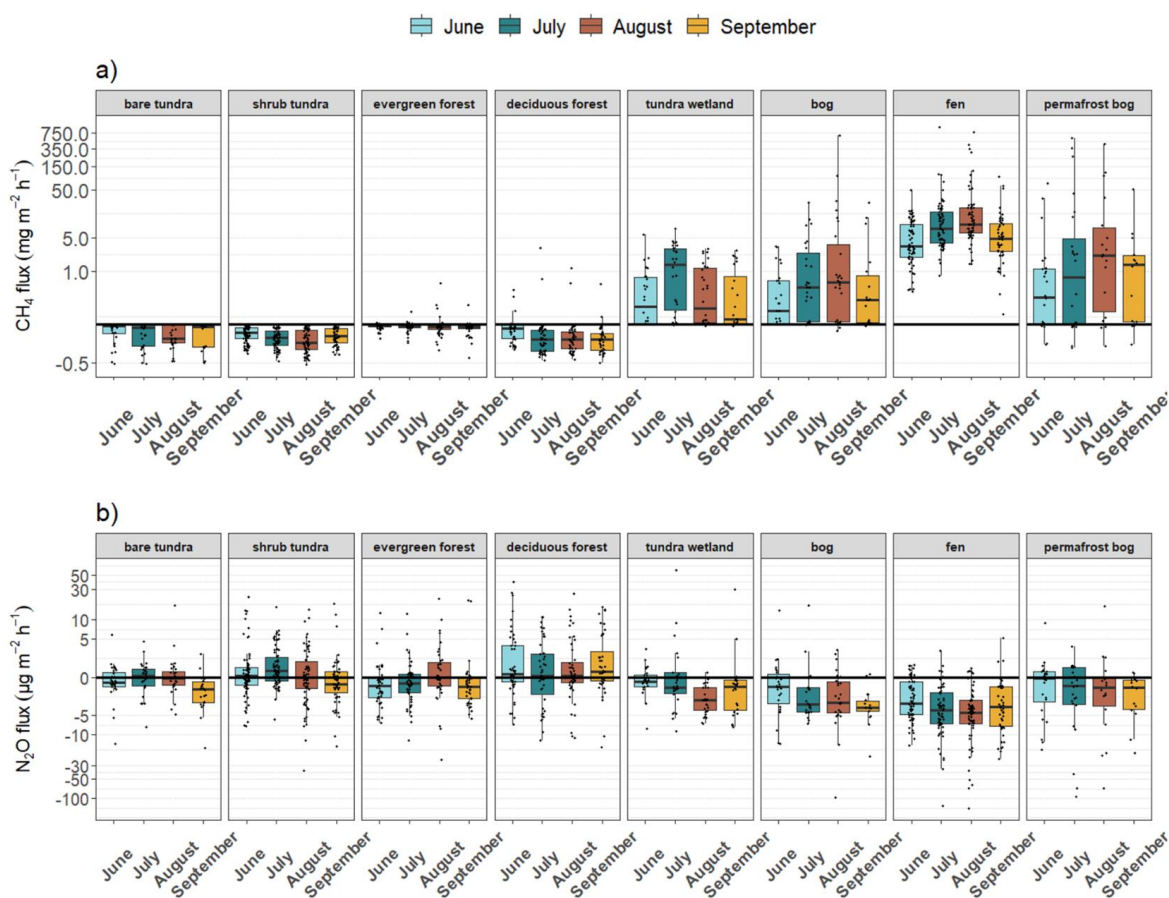


Figure 2. Growing season variability of CH<sub>4</sub> and N<sub>2</sub>O (both log<sub>10</sub>-transformed) in the eight land cover classes, positive values are emissions and negative values are sinks. Boxplots have 25<sup>th</sup> and 75<sup>th</sup> quantiles, median (horizontal line), 1.5 IQR from the lower and higher quantiles (whiskers) and individual data points (black dots). Statistically significant differences between months can be found in Table A5 and A6.

332

333



### 334 **3.2 N<sub>2</sub>O between land cover classes**

335 N<sub>2</sub>O showed high variance within land cover classes, with fluxes ranging from -141 to 59.5  
336  $\mu\text{g m}^{-2} \text{h}^{-1}$  across all sites. Notably, all wetland types were on average, net sinks of N<sub>2</sub>O,  
337 although all land covers exhibited both positive and negative fluxes (Fig. 2b). Positive mean  
338 N<sub>2</sub>O fluxes were observed in deciduous forests (mean  $1.70 \mu\text{g m}^{-2} \text{h}^{-1}$ ; range  $-15.6$  to  $39.2$ )  
339 and shrub tundra ( $0.44 \mu\text{g m}^{-2} \text{h}^{-1}$ ;  $-36.9$  to  $23.0$ ). The strongest negative mean fluxes (net  
340 sinks) occurred in fens ( $-6.53 \mu\text{g m}^{-2} \text{h}^{-1}$ ;  $-142$  to  $5.13$ ) and permafrost bogs ( $-5.40 \mu\text{g m}^{-2}$   
341  $\text{h}^{-1}$ ;  $-92.8$  to  $16.6$ ). N<sub>2</sub>O sinks were also measured in bogs ( $-3.51 \mu\text{g m}^{-2} \text{h}^{-1}$ ), tundra  
342 wetlands ( $-0.89 \mu\text{g m}^{-2} \text{h}^{-1}$ ), bare tundra ( $-0.69 \mu\text{g m}^{-2} \text{h}^{-1}$ ), and evergreen forests ( $-0.52 \mu\text{g}$   
343  $\text{m}^{-2} \text{h}^{-1}$ ).

344 Mean CH<sub>4</sub> and N<sub>2</sub>O fluxes were significantly inversely correlated (Spearman  $R = -0.70$ ,  $p <$   
345  $0.001$ ), with positive CH<sub>4</sub> fluxes generally associated with strong negative N<sub>2</sub>O fluxes (sinks).

### 346 **3.21 N<sub>2</sub>O Temporal trends**

347 Unlike CH<sub>4</sub>, most land cover classes showed no significant trends between months for N<sub>2</sub>O  
348 (Table A6.) However, there was a significant difference in N<sub>2</sub>O fluxes between years, where  
349 year 2025 had smaller positive N<sub>2</sub>O fluxes and larger negative fluxes (Fig. 7). Furthermore,  
350 within plot variability was often very high and some plots would measure both negative and  
351 positive fluxes in monthly repeated measurements.

### 352 **3.4 Environmental variables**

353 Soil temperature during the conducted chamber measurements varied between  $-0.02$  and  
354  $22.18 \text{ }^\circ\text{C}$  (mean  $10.23 \text{ }^\circ\text{C}$ ). September was the coldest month with the exceptions of  
355 evergreen forests, deciduous forests and permafrost bogs, where the coldest month was June.  
356 Mean soil temperatures peaked in July or August depending on the land cover (Fig. 3b), with  
357 the highest single measurements generally occurring during August. Soil moisture varied  
358 between  $4.7\%$  and  $60.7\%$  across all plots. Mean soil moisture was highest in fens ( $56.5\%$ ),  
359 followed by tundra wetlands ( $55.4\%$ ), bogs ( $40.8\%$ ), permafrost bogs ( $34.2\%$ ), evergreen  
360 forests ( $32.5\%$ ), deciduous forests ( $31.9\%$ ), shrub tundra ( $26.9\%$ ) and bare tundra ( $25.2\%$ ).  
361 Generally, soil moisture was highest in June due to snow melt waters and then steadily  
362 dropped towards August. Depending on the land cover, August or September was generally  
363 the driest month (Fig. 3a). Green vegetation cover ranged from  $0.01\%$  to  $85.6\%$ , with mean  
364 values highest in deciduous forest ( $37.5\%$ ) and lowest in bare tundra ( $3.2\%$ ); other land



365 covers fell between 12–25%. Green vegetation cover peaked in July or August depending on  
366 the land cover while the lowest values were recorded in June and September (Fig. 3c.). Soil  
367 pH was very acidic across all plots except for a few small areas with dolomite runoff. Mean  
368 pH was highest in tundra wetlands (5.53), followed by bare tundra (5.21), deciduous forests  
369 (5.07), fens (4.85), shrub tundra (4.53), bogs (4.45), evergreen forests (4.38) and permafrost  
370 bogs (4.12) (Fig. 3d).

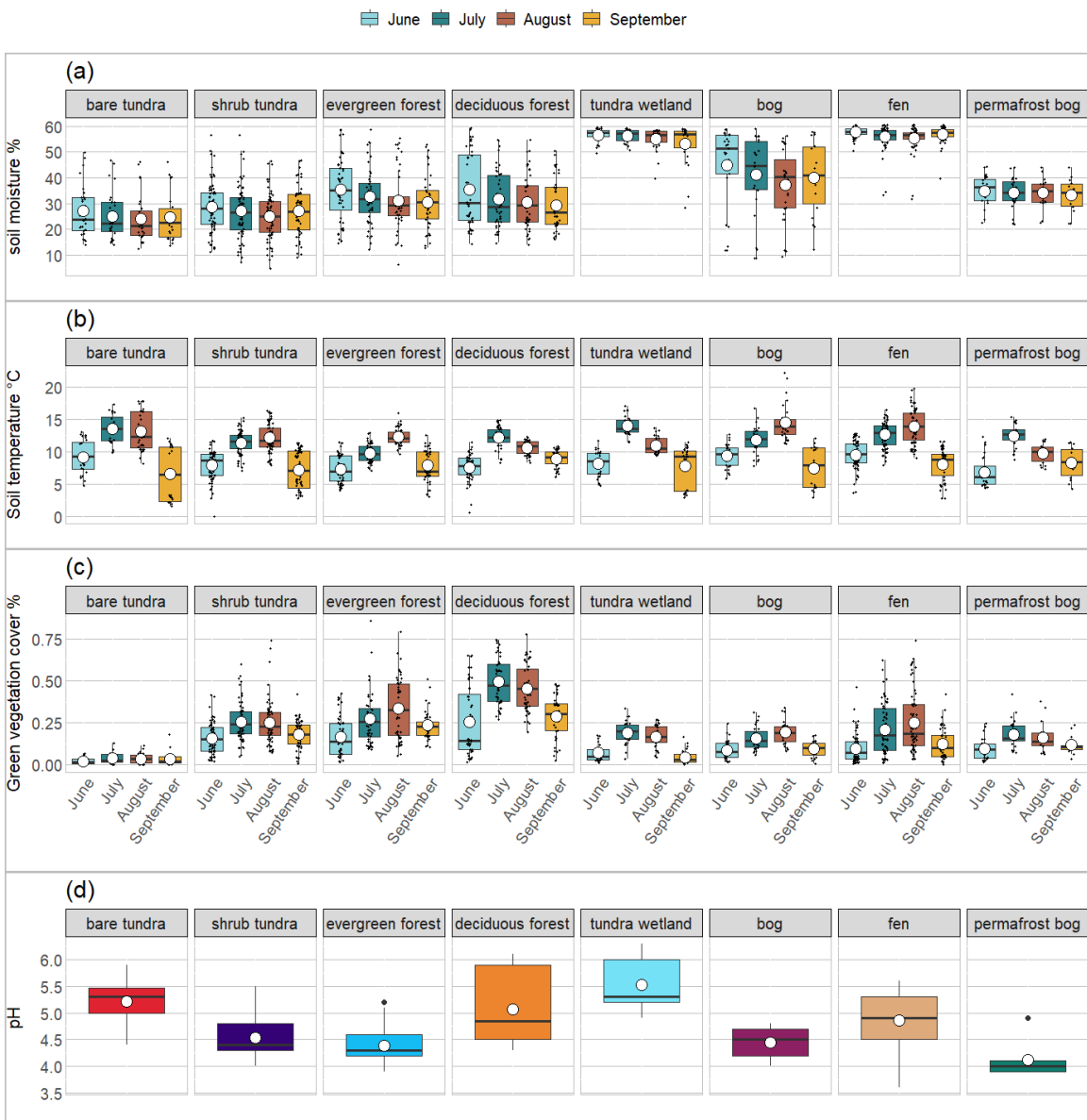


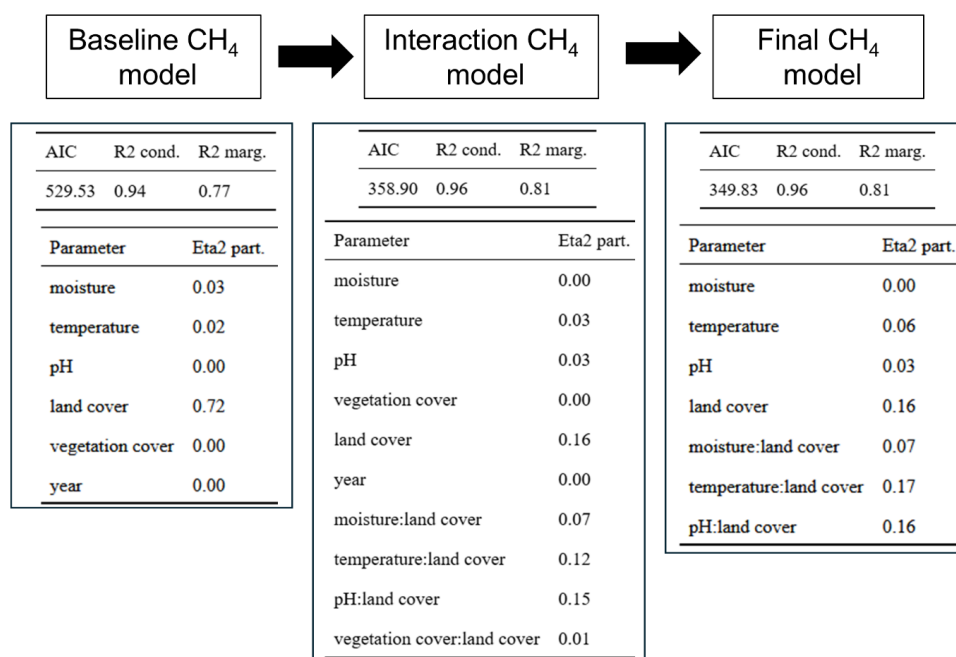
Figure 3. Variation in soil and vegetation characteristic. Boxplots of a) soil moisture, b) soil temperature and c) green vegetation cover between different land covers and months and d) pH between land covers. Boxplots have 25th and 75th quantiles, median (horizontal line), mean (white dot), 1.5 IQR from the lower and higher quantiles (whiskers).



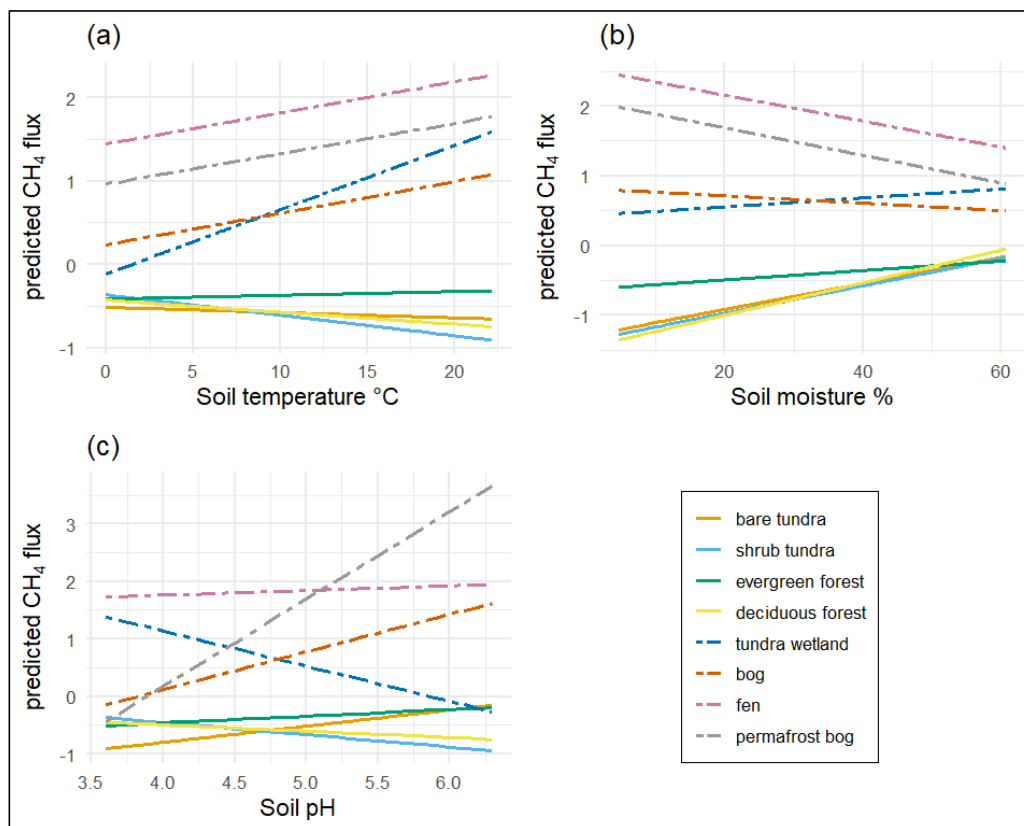
372 **3.5 Multivariate models**

373 **3.51 CH<sub>4</sub>**

374 The mixed-effects model for CH<sub>4</sub> showed high explanatory power (R<sup>2</sup> cond. = 0.96, R<sup>2</sup>  
 375 marg. 0.81). Moisture, temperature and pH all influenced CH<sub>4</sub> fluxes, however the direction  
 376 of the response was dependent on the land cover (Fig. 5). Highest effect variables based on  
 377 partial eta-squared ( $\eta^2_p$ ) were soil temperature (interaction) and pH (interaction) (Fig. 4, final  
 378 model). For land cover main effect, the CH<sub>4</sub> fluxes were highest in fens, followed by bogs,  
 379 permafrost bogs, tundra wetlands, evergreen forests, bare tundra, shrub tundra and deciduous  
 380 forests (Table A3). All non-wetland land cover classes modelled as net sinks (negative  
 381 fluxes).



382  
 383 *Figure 4. Model performance indicators for the CH<sub>4</sub> linear Mixed-Effects Models. The*  
 384 *baseline model, which included only main effects, showed lower explanatory power*  
 385 *compared to the interaction model that incorporated interactions with land cover class.*  
 386 *The final model was obtained after removing the least influential predictors based on*  
 387 *AIC to achieve a more parsimonious model structure. Partial eta-squared (Eta2 part.)*  
 388 *describes the effect size of each model parameter.*



389

390 *Figure 5. Land cover specific modelled (linear mixed-effect model) responses of CH<sub>4</sub> to*  
391 *a) soil temperature, b) soil moisture, c) pH. All CH<sub>4</sub> model variables included interaction*  
392 *terms, so no simple main effects are shown. Dashed lines represent wetlands.*



393 **3.52 N<sub>2</sub>O**

394 The mixed-effects model for N<sub>2</sub>O showed modest explanatory power (R<sup>2</sup> cond. = 0.38, R<sup>2</sup>  
 395 marg. = 0.30, fig 6.). Modelled N<sub>2</sub>O fluxes were highest in deciduous forests, followed by  
 396 shrub tundra, bare tundra, evergreen forests, tundra wetlands, bogs, fens and permafrost bogs  
 397 (fig 7.). Land cover and its interaction with pH were the strongest predictors while both soil  
 398 moisture and temperature had noticeably less effect (fig 6.). Unlike CH<sub>4</sub>, years 2024 and  
 399 2025 also showed a noticeable difference for N<sub>2</sub>O with 2025 generally having smaller  
 400 positive fluxes and larger sinks (fig 7.). In addition, vegetation cover had a small but  
 401 significant effect on N<sub>2</sub>O fluxes depending on the land cover type (fig 7.). The point  
 402 identification random effect also had a weaker effect compared to the CH<sub>4</sub> model.

403

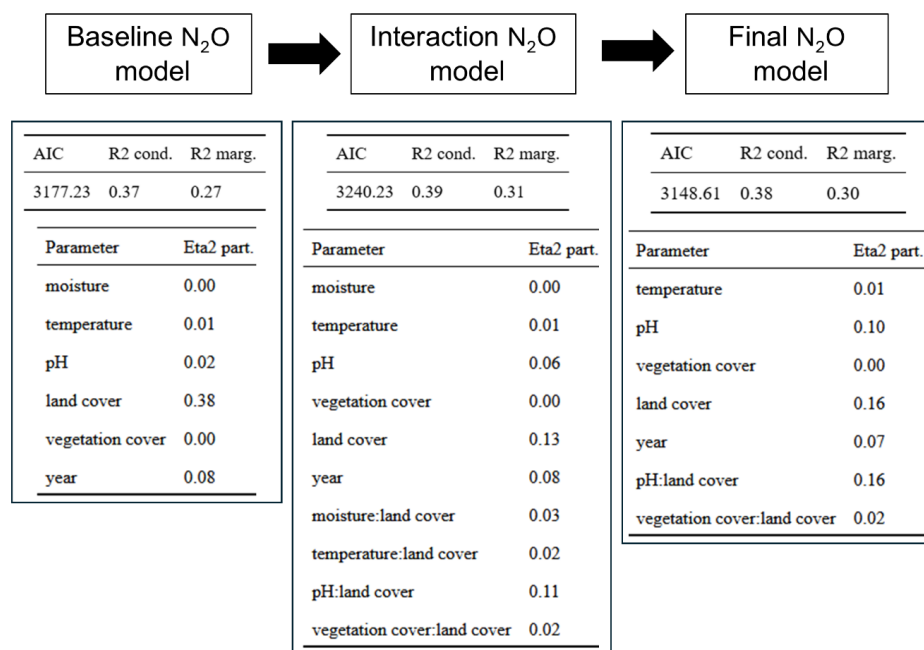


Figure 6. Model performance indicators for the N<sub>2</sub>O linear mixed-effects models. The baseline model, which included only main effects, showed lower explanatory power compared to the interaction model that incorporated interactions with land cover class. The final model was obtained after removing the least influential predictors based on AIC to achieve a more parsimonious model structure. Partial eta-squared (Eta2 part.) describes the effect size of each model parameter.



404

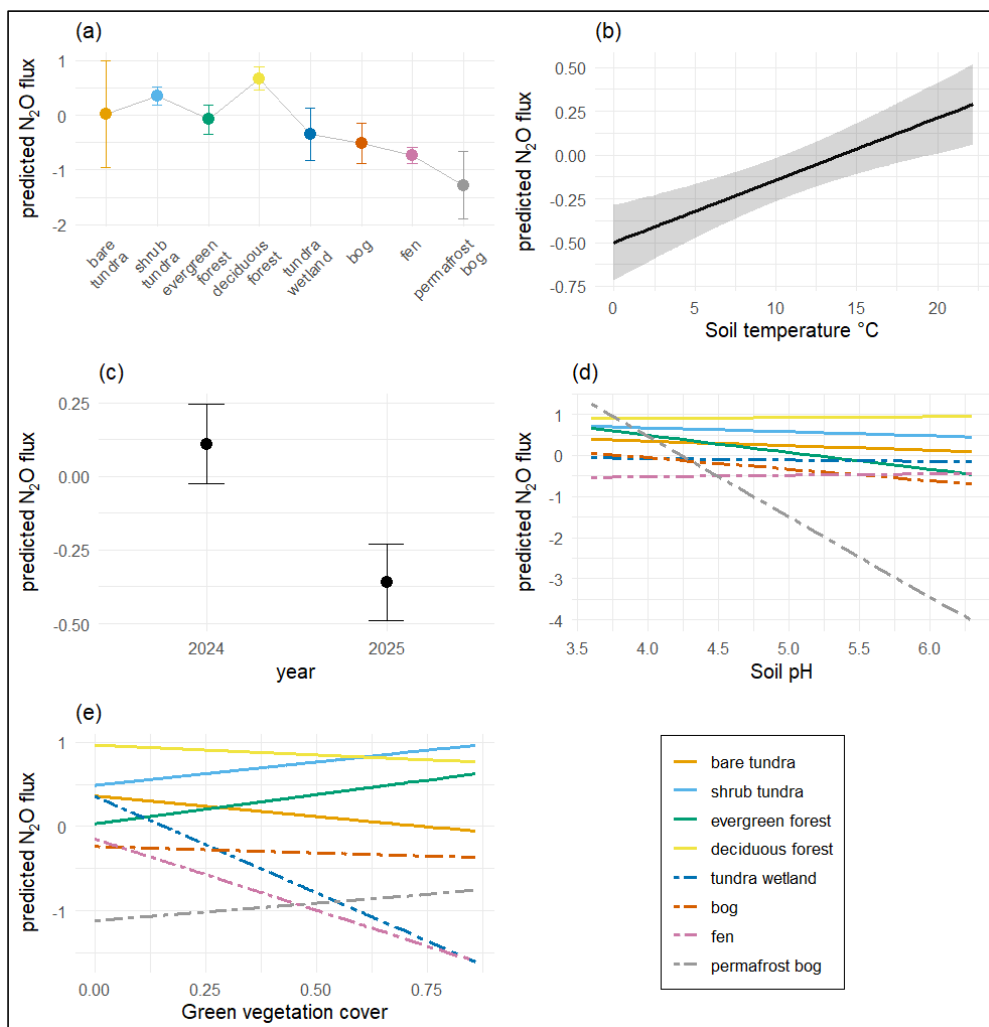


Figure 7. Modelled (linear mixed-effects model) responses of N<sub>2</sub>O to a) land cover, b) soil temperature, c) year, d) pH-land cover interaction and e) green vegetation cover-land cover interaction. Note differences in the scale of y-axis between subfigures. Dashed lines represent wetlands.



405

406

## 4. Discussion

407

Our findings on the seasonal and spatial patterns of CH<sub>4</sub> and N<sub>2</sub>O fluxes provide several insights into how environmental drivers shape gas exchange across high-latitude subarctic and boreal landscapes. The strongest predictors for GHG fluxes were soil temperature and pH, with the direction and strength of the responses changing based on land cover.

408

409

410

411

### 4.1 GHG flux magnitudes

412

Forest and dry tundra sites acted as net CH<sub>4</sub> sinks (-0.16 to -0.05 mg m<sup>-2</sup> h<sup>-1</sup>, depending on land cover class) and as both N<sub>2</sub>O sources and sinks (-0.69 to 1.69 μg m<sup>-2</sup> h<sup>-1</sup>). Wetlands were net CH<sub>4</sub> sources (0.93 to 27.81 mg m<sup>-2</sup> h<sup>-1</sup>) and net N<sub>2</sub>O sinks (-0.89 to -6.53 μg m<sup>-2</sup> h<sup>-1</sup>), with fens and permafrost bogs having the highest CH<sub>4</sub> fluxes and largest N<sub>2</sub>O sinks (see full descriptions of GHG magnitudes in Table A1 and A2).

413

414

415

416

417

Overall, the wetland CH<sub>4</sub> emissions were quite high but within maximum ranges reported in published literature (Turetsky et al., 2014; Tupek et al., 2015; Bao et al., 2021; Kuhn et al., 2021; Virkkala et al., 2025, preprint). Similar to our measurements, the ABCFlux CH<sub>4</sub> database (Virkkala et al., 2025, preprint) also had peak fluxes in August. Our forest and tundra CH<sub>4</sub> sinks were larger (more negative) than many previously reported values (Emmerton et al., 2014; Voigt et al., 2023; Virkkala et al., 2025, preprint), where some studies have even reported positive fluxes from upland tundra soils (Kuhn et al., 2021). Also, our mean net CH<sub>4</sub> sinks peaked in August, whereas in the ABCFlux database CH<sub>4</sub> sinks peaked in July (Virkkala et al., 2025, preprint). Our N<sub>2</sub>O sources were generally at the lower end of the reported ranges, while the N<sub>2</sub>O sinks were at the higher end (more negative) (Repo et al., 2009; Lohila et al., 2010; Maruschack et al., 2011; Tupek et al., 2015; Voigt et al., 2020; Virkkala et al., 2024; Triches et al., 2025, preprint).

418

419

420

421

422

423

424

425

426

427

428

429

### 4.2 Environmental drivers of CH<sub>4</sub>

430

We observed that CH<sub>4</sub> emissions increased with higher soil moisture across most of the study sites. This pattern is consistent with the underlying microbial processes: methanogenesis occurs primarily in anaerobic soils, whereas methanotrophy dominates under aerobic conditions. Soil oxygen content follows soil water content and as such soil moisture should have a direct causal effect on CH<sub>4</sub> emissions. Our results show that in non-wetland

431

432

433

434



435 soils, soil moisture was a good indicator for CH<sub>4</sub>. The few positive CH<sub>4</sub> measurements in  
436 non-wetland soils (Fig. 2a) were always from ecotones close to wetlands or streams or  
437 because of spring snow melt waters saturating the soils for extended periods of time.  
438 Conversely, CH<sub>4</sub> sinks in dry soils also grew stronger (more negative) with decreasing soil  
439 moisture. Notably, all mean and median fluxes for CH<sub>4</sub> in non-wetland environments were  
440 negative. Christiansen et al. (2015), Voigt et al. (2023) and Virkkala et al. (2024) reported  
441 similar findings, with soil moisture being one of the major drivers for CH<sub>4</sub> sinks at high-  
442 latitude dry upland soils and Lohila et al. (2016) found that a prolonged wet autumn period  
443 changed a net CH<sub>4</sub> sink forest into a net source for several months. Although the CH<sub>4</sub> sinks  
444 are relatively small when compared to wetland emissions, dry tundra and boreal forest soils  
445 cover extensive areas of the northern hemisphere which leads to a globally significant CH<sub>4</sub>  
446 sink (Jiang et al., 2025), and as previously mentioned (see 4.1), the sink magnitudes reported  
447 here are larger than in many previous studies. The soil CH<sub>4</sub> sink is still poorly constrained in  
448 global CH<sub>4</sub> budgets (Saunois et al., 2025) and should be considered in further studies.

449 In wetland environments, soil moisture has a more complex relationship to CH<sub>4</sub>.  
450 Often the wetland types with highest soil moisture (i.e. fens and marshes) are also the highest  
451 CH<sub>4</sub> emitters (Kuhn et al., 2021), however within those wetland types, increased soil  
452 moisture does not necessarily increase CH<sub>4</sub> flux (Knox et al., 2019). Our results show that,  
453 within the different fen sites, the wettest soils were not the largest emitters (Fig. 5b). Soil  
454 moisture also did not increase CH<sub>4</sub> emissions in bogs or permafrost bogs. In permafrost bogs  
455 (palsas), intact palsas exhibited higher soil moisture but acted as substantially smaller CH<sub>4</sub>  
456 sources compared to fully degraded ones. This suggests that additional factors, such as soil  
457 pH, vegetation, or active layer thickness, may play a more important role in regulating  
458 wetland CH<sub>4</sub> fluxes. Similar results were reported by Turetsky et al. (2014) and Rinne et al.  
459 (2018), who found that CH<sub>4</sub> fluxes were smaller in fully flooded wetland soils and that higher  
460 water-table levels alone did not predict higher fluxes in boreal fens. Generally, in wetlands  
461 there is likely an upper threshold of optimal moisture conditions for methanogenesis after  
462 which soil moisture no longer increases CH<sub>4</sub> flux. Reduced CH<sub>4</sub> emissions at sites with  
463 extreme soil moisture are likely the result of differences in substrate availability (i.e. less  
464 labile organic material) and temperature regime (Strack et al., 2004).

465 Soil temperature and land cover interaction was the strongest predictor for CH<sub>4</sub> fluxes  
466 (Fig. 4) and soil temperature has been identified as a key driver of CH<sub>4</sub> fluxes in many  
467 previous studies (Turetsky et al., 2014; Knox et al., 2019; Kuhn et al., 2021; Kübert et al.,



468 2026). Soil temperature directly affects both methanogenesis and methanotrophy as they are  
469 microbial processes and therefore causally linked to soil temperature through the  
470 temperature-dependence of microbial activity (Moore and Dalva 1993; Biasi et al., 2005;  
471 Deslippe et al., 2012). This also indicates that rising temperatures can intensify CH<sub>4</sub>  
472 dynamics in opposite directions where the net effect on emissions is dependent on the  
473 ecosystem's temperature sensitivity (Zhang et al., 2021). This effect can also be seen in our  
474 modelled CH<sub>4</sub> flux responses (Fig. 5a), where wetland CH<sub>4</sub> fluxes have a positive response to  
475 higher temperatures and non-wetland soils have a negative response, with higher  
476 temperatures leading to larger sinks (i.e. net-sink environments become stronger sinks and  
477 net-source environments emit more CH<sub>4</sub>). Additionally, warming can affect the amount of  
478 organic material available for decomposition through increased GPP as higher mean  
479 temperatures generally increase biomass which could further enhance CH<sub>4</sub> fluxes (Knox et  
480 al., 2021). Thus, rising temperatures under climate change can strengthen both CH<sub>4</sub> sinks and  
481 CH<sub>4</sub> sources depending on land cover type, meaning that long-term changes in net CH<sub>4</sub>  
482 emissions will depend largely on shifts in land cover and ecosystem distributions and their  
483 effects on soil conditions.

484 Soil pH had a strong but mixed influence on CH<sub>4</sub> fluxes depending on land cover type  
485 (Fig. 5c). This response appeared to be related to the overall pH of these environments.  
486 Low-pH systems, such as permafrost bogs, bogs, and evergreen forests (Fig. 4d), showed a  
487 positive response to increasing pH, meaning higher CH<sub>4</sub> fluxes. In contrast, higher-pH  
488 environments, such as tundra wetlands and deciduous forests, showed the opposite pattern,  
489 meaning smaller fluxes with increased pH. It is worth noting that overall, all our  
490 measurement sites would typically be classified as acidic since the overall pH range is  
491 between 3.6–6.3 and as such, most vegetation and soil biota, including microbes, are adapted  
492 to acidic conditions (Kip et al., 2011, Yao et al., 2023). At the lower end of that pH range,  
493 most plant species and microbes likely exist at the far end of their acidity tolerance (Yao et  
494 al., 2023) and even small increases in pH could increase their overall activity. This may  
495 explain the strong response seen in bogs and permafrost bogs as pH increases. At the opposite  
496 end, some of the tundra wetland and deciduous forest sites are affected by dolomite runoff  
497 from the surrounding watershed which significantly increases the overall soil pH. At these  
498 sites a higher pH decreased the CH<sub>4</sub> flux (Fig. 5c), which could indicate that methanogenesis  
499 is inhibited by higher pH while methanotrophs benefit from it. Conversely, it could also be a  
500 result of methanogenetic Archaea being more tolerant of acidic conditions than



501 methanotrophs (Weslien et al., 2009). Other factors could also be of importance, specifically  
502 nutrient availability and vegetation are partly controlled by soil pH and directly affect CH<sub>4</sub>  
503 dynamics. Nonetheless, pH can exert a strong effect on CH<sub>4</sub> fluxes and should be considered  
504 in further studies.

#### 505 **4.3 Environmental drivers of N<sub>2</sub>O**

506 Similarly to CH<sub>4</sub> production and consumption, N<sub>2</sub>O dynamics are also governed by  
507 microbial processes and are therefore influenced by factors such as soil temperature,  
508 moisture, pH, and vegetation. N<sub>2</sub>O is mostly produced in the denitrification process where  
509 nitrates are reduced back into N<sub>2</sub> (Butterbach-Bahl et al., 2013). Other possible, but less  
510 important pathways include nitrification and nitrate/nitrite reduction to ammonium. Soil  
511 oxygen content has a causal link to N<sub>2</sub>O flux as nitrification generally only occurs in aerobic  
512 conditions and denitrification and reduction to ammonium mostly occur in anaerobic  
513 conditions (Shan et al., 2021). However, N<sub>2</sub>O showed a much weaker response to the  
514 environmental variables compared to CH<sub>4</sub>, and the explanatory power of the models was  
515 correspondingly smaller (Fig. 4 and Fig. 6). In addition, N<sub>2</sub>O showed a significant difference  
516 between measurement years which remained unexplained by the other factors, suggesting that  
517 some key explanatory variables were missing from the model.

518 Previous studies have identified sources of N<sub>2</sub>O from many high-latitude  
519 environments such as unvegetated permafrost peat plateaus and palsas (Maruschak et al.,  
520 2011) and both vegetated and unvegetated permafrost tundra soils (Voigt et al., 2020) but  
521 also sinks from nutrient-poor permafrost peatlands (Triches et al., 2025, preprint) and  
522 grasslands and forests (Chapuis-Lardy et al., 2007). In our measurements, we found strong  
523 sinks from wetlands, while non-wetland environments had medians close to zero fluxes,  
524 however there was a noticeable amount of both negative and positive extreme values (Fig.  
525 2b) and many land cover classes and single measurement plots exhibited both negative and  
526 positive fluxes. This type of flux behaviour is not uncommon (Lohila et al., 2010; Tupek et  
527 al., 2015) and highlights the spatiotemporally sporadic behaviour of N<sub>2</sub>O, where many plots  
528 have zero or small positive N<sub>2</sub>O emissions, yet a small number of plots can act as significant  
529 hotspots, both for sinks and sources (Maruschak et al., 2011; Triches et al., 2025, preprint).

530 Soil temperature and moisture generally had modest effects on N<sub>2</sub>O fluxes and much  
531 of the variability was explained by pH and land cover (particularly wetlands). Our highest  
532 measured mean fluxes came from deciduous (mountain birch) forests, which also had



533 comparatively higher soil pH (Fig. 3d). Cryoturbation and the absence of vegetation have  
534 been occasionally reported as having an increasing effect on N<sub>2</sub>O fluxes, especially in  
535 permafrost soils (Repo et al., 2009; Maruschak et al., 2011; Voigt et al., 2020). However, we  
536 found no strong evidence for such an effect in our measurements from peat soils or tundra  
537 cryoturbation plots. Both bare tundra and permafrost bogs acted as small net sinks for N<sub>2</sub>O  
538 (Fig. 2b), and vegetation cover only had a small effect in the model results.

539 It is possible that low soil nitrogen availability is the primary reason for the small N<sub>2</sub>O  
540 fluxes, while also being a key missing variable in the model. Nitrate (NO<sub>3</sub><sup>-</sup>) and nitrite (NO<sub>2</sub><sup>-</sup>)  
541 are the preferred electron acceptors in denitrification, thus in the presence of excess soil  
542 nitrogen content, N<sub>2</sub>O would not be reduced and would likely result in larger positive fluxes.  
543 Furthermore, there is evidence of NO<sub>3</sub><sup>-</sup> reliant pathways of methanotrophy that can produce  
544 N<sub>2</sub>O in low oxygen conditions such as wetlands (Kits et al., 2015).

#### 545 **4.4 N<sub>2</sub>O sinks**

546 The largest N<sub>2</sub>O sinks were found in wetlands, specifically in fen plots (Fig. 2b). This  
547 may appear counterintuitive as denitrification, which is the main pathway for N<sub>2</sub>O production  
548 (Butterbach-Bahl et al., 2013), requires anoxic conditions which wetlands typically have. The  
549 reason is likely in the last step of the denitrification chain where N<sub>2</sub>O is reduced. In anoxic  
550 conditions with high C/N ratios or low NO<sub>3</sub><sup>-</sup> concentrations, the denitrification process is  
551 fully completed, N<sub>2</sub>O is produced but then reduced into N<sub>2</sub> gas (Kolb & Horn 2012, Brummel  
552 et al., 2012, Pessi et al., 2022). In these low-nitrate conditions, any excess N<sub>2</sub>O would be  
553 rapidly reduced, including atmospheric N<sub>2</sub>O, resulting in a net sink.

554 Other less studied pathways for N<sub>2</sub>O sinks and the inverse N<sub>2</sub>O and CH<sub>4</sub> correlation  
555 involve anaerobic methane oxidation driven by denitrification (Valenzuela 2020, Tan et al.,  
556 2025). It follows that in soils rich in CH<sub>4</sub>, such as wetlands, substantial methanotrophic  
557 activity would occur throughout the soil profile, provided that environmental conditions  
558 permit it (Whalen et al., 1990). However, chamber measurements only capture the net CH<sub>4</sub>  
559 flux, so if net oxidation is smaller than net CH<sub>4</sub> production, the oxidation would not be  
560 detected. Anaerobic methane oxidation (AOM) is a well-known process in marine  
561 environments (Hinrichs & Boetius 2002, Reeburgh 2007), but less so in wetlands, yet there is  
562 growing evidence for its importance (Smemo and Yavitt 2011, Cai et al., 2019, Cheng et al.,  
563 2021). In AOM, CH<sub>4</sub> can be used as electron donor for reducing nitrite and N<sub>2</sub>O, which  
564 would act as an additional sink of N<sub>2</sub>O (Valenzuela et al., 2020, Cheng et al., 2021, Tan et al.,



565 2025). However, the magnitude of these pathways in natural systems is unknown and  
566 somewhat hypothetical at this point and needs more research to be confirmed. Regardless of  
567 the underlying mechanisms, based on our measurements, wetlands can act as a notable N<sub>2</sub>O  
568 sinks in the right conditions.

569

## 570 **5. Uncertainties**

571 The monthly repeated measurements and two-year design resulted in a robust overall dataset,  
572 even though some land cover classes, such as permafrost bogs, were represented by fewer  
573 plots. Generic environmental variables that can be measured from anywhere make the models  
574 easily applicable everywhere, but it also limits the number of usable explanatory variables.  
575 Modelling across diverse environments (i.e. not solely focusing on specific ecosystems such  
576 as wetlands) provides a valuable opportunity to capture a wide range of ecosystem behaviors,  
577 though it naturally results in more complex data structures. In particular, wetland GHG fluxes  
578 often show substantial variability, including occasional high fluxes far above median values  
579 (Kuhn et al., 2021; Saunio et al., 2024). These contrasts become pronounced when wetlands  
580 and non-wetland systems are analyzed together due to their inherently different flux  
581 magnitudes. Furthermore, capturing seasonal changes requires repeated measurements which  
582 limit the available statistical methods due to pseudoreplication. These complexities were  
583 effectively addressed in our statistical analyses through the use of robust and flexible  
584 approaches, including mixed multivariate models, appropriate data transformations, and  
585 non-parametric tests.

586 The multivariate and correlative nature of our models makes it challenging to directly  
587 disentangle causal pathways. Also, some variables, such as land cover, function as a  
588 composite descriptor of multiple co-varying environmental conditions rather than a direct  
589 mechanistic driver. Because land cover classes ultimately reflect underlying temperature,  
590 moisture, and other soil properties, these environmental factors are the more direct drivers of  
591 GHG fluxes than land cover per se.

592 Opaque (“dark”) chambers are used to reduce uncertainties caused by changes in  
593 chamber temperature or possible interactions between photosynthesis and GHG fluxes and  
594 are typically the default method for measuring CH<sub>4</sub> and N<sub>2</sub>O fluxes (Livingston &  
595 Hutchinson, 2009; Pavelka et al., 2018; Clough et al., 2020). However, there is recent  
596 evidence of CH<sub>4</sub> and N<sub>2</sub>O fluxes being affected by varying light conditions (Voigt et al.,



597 2023; Triches et al., 2025, preprint). Thus, it is possible that GHG fluxes measured with  
598 transparent and opaque chambers are not directly comparable and the additional use of  
599 transparent chambers should be considered in future research.

600

## 601 **6. Conclusions**

602 Across all ecosystems, we found consistent contrasts in greenhouse gas dynamics, with  
603 tundra and forest sites acting as modest CH<sub>4</sub> sinks and wetlands functioning as strong CH<sub>4</sub>  
604 sources, whereas N<sub>2</sub>O flux patterns were more subtle. Most notably wetlands acted as  
605 consistent N<sub>2</sub>O sinks.

606 Land cover, pH, soil temperature and soil moisture were strong predictors of CH<sub>4</sub>  
607 fluxes and explained most of the observed variance, whereas vegetation cover had only a  
608 marginal effect. CH<sub>4</sub> fluxes exhibited clear seasonal patterns, with the smallest sources and  
609 sinks occurring at the beginning and end of the growing season while peak fluxes were  
610 observed in July–August. These findings highlight the importance of longitudinal studies for  
611 accurately estimating annual CH<sub>4</sub> budgets rather than relying solely on peak growing-season  
612 measurements but also demonstrates that CH<sub>4</sub> fluxes can be modelled with relatively few key  
613 environmental variables.

614 In comparison to CH<sub>4</sub>, N<sub>2</sub>O exhibited relatively moderate responses to the measured  
615 environmental variables and considerably weaker seasonal patterns, emphasizing the inherent  
616 challenges in explaining N<sub>2</sub>O dynamics across heterogeneous ecosystems. In a multivariate  
617 context, land cover and soil pH emerged as the most influential factors shaping N<sub>2</sub>O flux  
618 variability, while the effects of soil temperature and moisture were negligible. The substantial  
619 proportion of unexplained variability in N<sub>2</sub>O fluxes indicates that key controlling factors were  
620 not fully captured, pointing to the importance of additional drivers, particularly those related  
621 to soil biogeochemistry and microbial nitrogen transformation pathways. Furthermore, the  
622 high variability of N<sub>2</sub>O emissions suggests a notable influence of spatiotemporal dynamics,  
623 underscoring the need for high resolution measurements to adequately characterize N<sub>2</sub>O  
624 behavior. These findings highlight the complexity of N<sub>2</sub>O dynamics and identify important  
625 avenues for future research to improve the understanding and modeling of N<sub>2</sub>O fluxes.

626 All in all, our results demonstrate that high-latitude GHG fluxes arise from  
627 interactions between broad land cover patterns and fine-scale environmental variability. From



628 an applied perspective, our findings suggest that accurate land cover mapping and *in situ*  
629 measurements of soil conditions are essential for robust modelling and upscaling of GHG  
630 fluxes. Because land cover classes exhibit such different GHG dynamics due to the  
631 underlying soil and vegetation characteristics, improved classification greatly enhances  
632 predictive performance across heterogenous landscapes. This is especially important in  
633 high-latitude regions, where rapid warming is expected to alter both ecosystem distributions  
634 and soil conditions with significant implications for current and future GHG budgets.

### 635 **Author contributions**

636 Conceptualization: ML, JH, JN, AMV; Methodology: ML, JN, JH, AMV; Formal analysis:  
637 JN; Investigation: JN, JL; Resources: JH, ML, AMV; Data curation: JN, JL; Writing -  
638 Original draft: JN; Writing - Review & Editing: JN, ML, JH, AMV, JL; Visualization: JN,  
639 JL; Supervision: ML, JH, AMV; Project administration: ML, JH, JN; Funding acquisition:  
640 JH, ML

### 641 **Competing Interests**

642 The authors declare that they have no conflict of interest.

### 643 **Code and data availability**

644 Data and R scripts used for the data visualizations and analysis can be provided by the  
645 corresponding authors upon request.

646 Python script for flux calculations available at [https://github.com/janivaltteri/manual-](https://github.com/janivaltteri/manual-chamber-dataserver/blob/main/dataserver/application/fluxcalc.py)  
647 [chamber-dataserver/blob/main/dataserver/application/fluxcalc.py](https://github.com/janivaltteri/manual-chamber-dataserver/blob/main/dataserver/application/fluxcalc.py)

### 648 **Acknowledgements**

649 The authors want to acknowledge and thank field assistants Leo Mäklin, Sara Solastie, Anna  
650 Liljefors, Lotta Mattila, Lea Fewer, Katariina Karvinen for field work in 2024 and 2025 as  
651 well as Kilpisjärvi biological station for providing facilities for our field campaigns. We also  
652 acknowledge Metsähallitus for research permits.

653 The authors used OpenAI's ChatGPT (GPT-5) for minor language editing and readability  
654 improvements. Additionally, ChatGPT was used to help troubleshoot R code and resolve  
655 coding errors during the creation of figures.

### 656 **Financial support**



657 This work was supported by Kone foundation (Uinuvat mikrobit to JH and ML) and  
658 Academy of Finland (project: 1342890 to ML, 354462 to JH and 371479 to AMV) and  
659 Nordenskiöld samfundet to JN and JL, Nesling foundation to JL, Waldermar von Freckell's  
660 stiftelse to AMV, Luke doctoral school travel funds to JN.



661 **Appendices**

662

663 *Table A1. CH<sub>4</sub> and N<sub>2</sub>O fluxes in different land cover classes*

land cover	CH <sub>4</sub> (mg m <sup>-2</sup> h <sup>-1</sup> )					N <sub>2</sub> O (µg m <sup>-2</sup> h <sup>-1</sup> )				
	Mean	SD	Median	Min	Max	Mean	SD	Median	Min	Max
bare tundra	-0.126	0.143	-0.075	-0.525	0.008	-0.691	3.354	-0.559	-16.101	16.721
shrub tundra	-0.160	0.097	-0.141	-0.553	0.001	0.435	4.774	0.191	-36.857	23.038
evergreen forest	-0.045	0.084	-0.042	-0.398	0.567	-0.523	4.491	-0.885	-24.271	21.549
deciduous forest	-0.123	0.298	-0.148	-0.499	3.020	1.697	6.484	0.574	-15.609	39.175
tundra wetland	0.925	1.354	0.245	-0.039	7.587	-0.893	7.241	-1.557	-8.772	59.463
bog	10.073	67.715	0.321	-0.108	668.329	-3.512	10.488	-2.942	-96.405	16.802
fen	23.368	90.651	6.561	0.128	1007.896	-6.527	14.321	-3.867	-141.854	5.134
permafrost bog	27.808	96.405	0.960	-0.242	602.251	-5.404	15.920	-1.034	-92.814	16.559

664

665

666 *Table A2. Monthly CH<sub>4</sub> and N<sub>2</sub>O fluxes in different land cover classes*

	land cover	CH <sub>4</sub> (mg m <sup>-2</sup> h <sup>-1</sup> )					N <sub>2</sub> O (µg m <sup>-2</sup> h <sup>-1</sup> )				
		Mean	SD	Median	Min	Max	Mean	SD	Median	Min	Max
<b>June</b>	bare tundra	-0.102	0.143	-0.040	-0.519	0.005	-0.900	3.251	-0.777	-13.855	5.774
	shrub tundra	-0.127	0.072	-0.119	-0.326	0.001	0.934	4.804	0.174	-7.323	23.038
	evergreen forest	-0.035	0.043	-0.022	-0.154	0.028	-0.966	3.249	-1.289	-6.440	12.971
	deciduous forest	-0.079	0.129	-0.087	-0.261	0.419	2.863	8.201	0.547	-6.835	39.175
	tundra wetland	0.643	1.213	0.197	0.001	5.940	-0.628	2.130	-0.725	-8.103	3.456
	bog	0.594	0.940	0.153	0.001	3.373	-1.734	5.109	-1.468	-13.851	13.886
	fen	6.433	7.366	3.321	0.385	49.585	-3.202	3.198	-3.198	-14.518	1.940
	permafrost bog	5.165	15.139	0.291	-0.211	68.058	-2.045	5.583	-0.170	-17.242	9.023
<b>July</b>	bare tundra	-0.133	0.150	-0.071	-0.525	0.005	-0.125	2.395	0.246	-7.636	4.548
	shrub tundra	-0.169	0.092	-0.149	-0.461	-0.001	1.441	3.062	1.068	-5.782	16.018
	evergreen forest	-0.048	0.058	-0.043	-0.188	0.147	-0.766	3.443	-0.906	-12.323	12.315
	deciduous forest	-0.104	0.510	-0.166	-0.453	3.020	0.603	5.080	0.274	-12.319	11.152
	tundra wetland	1.784	1.877	1.392	-0.012	7.587	1.300	12.380	-1.552	-8.772	59.463
	bog	2.877	5.801	0.470	-0.018	26.812	-2.074	4.438	-3.353	-6.650	16.802
	fen	28.840	121.145	7.639	0.812	1007.896	-7.364	16.234	-4.116	-130.475	3.297
	permafrost bog	54.310	145.913	1.009	-0.242	602.251	-9.334	23.795	-1.404	-92.814	3.859
<b>August</b>	bare tundra	-0.151	0.132	-0.156	-0.457	0.003	0.254	3.742	-0.207	-4.784	16.721
	shrub tundra	-0.197	0.119	-0.189	-0.553	-0.003	-0.274	6.011	-0.062	-36.857	14.503
	evergreen forest	-0.037	0.133	-0.058	-0.280	0.567	0.401	6.216	-0.011	-24.271	21.549
	deciduous forest	-0.145	0.240	-0.164	-0.425	1.160	1.244	6.053	0.260	-11.271	25.924
	tundra wetland	0.700	0.921	0.180	-0.039	2.948	-3.012	1.845	-2.885	-6.702	0.794
	bog	31.463	128.687	0.594	-0.108	668.329	-6.077	18.389	-3.189	-96.405	3.418
	fen	46.033	123.948	9.556	1.432	794.017	-10.279	21.438	-4.460	-141.854	1.425
	permafrost bog	40.396	107.838	2.140	-0.223	450.080	-6.032	17.471	-1.609	-68.213	16.559
<b>September</b>	bare tundra	-0.118	0.154	-0.053	-0.507	0.008	-2.350	3.566	-1.868	-16.101	2.884
	shrub tundra	-0.142	0.081	-0.140	-0.341	-0.003	-0.597	4.515	-1.028	-15.010	17.925
	evergreen forest	-0.060	0.084	-0.048	-0.398	0.200	-0.598	4.897	-1.417	-5.606	19.983
	deciduous forest	-0.170	0.160	-0.165	-0.499	0.540	2.019	5.964	0.929	-15.609	15.651
	tundra wetland	0.579	0.870	0.102	-0.035	2.700	-0.907	7.221	-1.499	-7.505	30.325
	bog	3.003	6.932	0.259	-0.038	26.535	-4.406	4.702	-3.730	-21.947	0.475
	fen	9.814	16.613	4.863	0.128	92.036	-5.119	5.880	-3.675	-24.178	5.134
	permafrost bog	5.008	13.228	1.375	-0.206	50.499	-3.617	5.547	-1.582	-19.359	0.707

667



668 *Table A3. Linear mixed-effects model summary for CH<sub>4</sub> flux. Model estimates are*  
 669 *standardized.*

**Linear mixed-effects model for CH<sub>4</sub> flux**

	<b>Est.</b>	<b>S.E.</b>	<b>t</b>	<b>p</b>
Intercept	-0.582	0.209	-2.786	0.005
moisture	0.284	0.092	3.102	0.002
temperature	-0.020	0.016	-1.232	0.218
pH	0.168	0.188	0.895	0.371
shrub tundra	-0.033	0.229	-0.143	0.886
evergreen forest	0.211	0.245	0.861	0.389
deciduous forest	0.004	0.232	0.018	0.986
tundra wetland	1.258	0.318	3.955	<0.001
bog	1.198	0.273	4.384	<0.001
fen	2.405	0.242	9.950	<0.001
permafrost bog	1.906	0.385	4.956	<0.001
moisture × shrub tundra	0.014	0.108	0.132	0.895
moisture × evergreen forest	-0.182	0.107	-1.704	0.089
moisture × deciduous forest	0.070	0.103	0.681	0.496
moisture × tundra wetland	-0.186	0.125	-1.489	0.137
moisture × bog	-0.365	0.106	-3.437	<0.001
moisture × fen	-0.568	0.121	-4.701	<0.001
moisture × permafrost bog	-0.585	0.160	-3.645	<0.001
temperature × shrub tundra	-0.057	0.022	-2.629	0.009
temperature × evergreen forest	0.034	0.025	1.358	0.175
temperature × deciduous forest	-0.025	0.029	-0.864	0.388
temperature × tundra wetland	0.264	0.028	9.462	<0.001
temperature × bog	0.140	0.027	5.154	<0.001
temperature × fen	0.138	0.022	6.229	<0.001
temperature × permafrost bog	0.135	0.032	4.268	<0.001
pH × shrub tundra	-0.295	0.220	-1.343	0.179
pH × evergreen forest	-0.099	0.240	-0.415	0.679
pH × deciduous forest	-0.234	0.205	-1.141	0.254
pH × tundra wetland	-0.535	0.239	-2.234	0.026
pH × bog	0.222	0.311	0.712	0.476
pH × fen	-0.120	0.204	-0.588	0.556
pH × permafrost bog	0.741	0.325	2.284	0.023

670



671 *Table A4. Linear mixed-effects model summary for CH<sub>4</sub> flux. Model estimates are*  
 672 *standardized.*

673

**Linear mixed-effects model for N<sub>2</sub>O Flux**

	<b>Est.</b>	<b>S.E.</b>	<b>t</b>	<b>p</b>
Intercept	0.265	0.499	0.531	0.595
temperature	0.113	0.027	4.176	<0.001
pH	-0.065	0.184	-0.354	0.723
vegetation cover	-0.078	0.457	-0.170	0.865
shrub tundra	0.334	0.506	0.661	0.509
evergreen forest	-0.091	0.518	-0.176	0.860
deciduous forest	0.653	0.512	1.275	0.202
tundra wetland	-0.366	0.555	-0.660	0.510
bog	-0.532	0.530	-1.004	0.316
fen	-0.753	0.504	-1.496	0.135
permafrost bog	-1.283	0.586	-2.189	0.029
year 2025	-0.471	0.048	-9.790	<0.001
pH × shrub tundra	0.007	0.215	0.035	0.972
pH × evergreen forest	-0.182	0.238	-0.765	0.444
pH × deciduous forest	0.078	0.200	0.388	0.698
pH × tundra wetland	0.043	0.235	0.185	0.853
pH × bog	-0.102	0.306	-0.334	0.738
pH × fen	0.086	0.202	0.427	0.669
pH × permafrost bog	-1.106	0.312	-3.544	<0.001
vegetation cover × shrub tundra	0.166	0.464	0.358	0.720
vegetation cover × evergreen forest	0.188	0.463	0.407	0.684
vegetation cover × deciduous forest	0.041	0.460	0.088	0.930
vegetation cover × tundra wetland	-0.286	0.486	-0.589	0.556
vegetation cover × bog	0.054	0.493	0.109	0.913
vegetation cover × fen	-0.191	0.461	-0.415	0.678
vegetation cover × permafrost bog	0.144	0.497	0.290	0.772

674

675



676 *Table A5. ART-ANOVA summary for monthly differences of CH<sub>4</sub> flux between land cover*  
 677 *types*

land cover	month	estimate	SE	df	t.ratio	p.value	sig
bare tundra	June- September	49.90	23.58	1095.29	2.12	0.97	
bare tundra	July- June	-65.93	22.07	1095.01	-2.99	0.42	
bare tundra	July- September	-16.03	23.58	1095.29	-0.68	1.00	
bare tundra	August- June	-130.79	22.07	1095.01	-5.93	0.00	***
bare tundra	August- July	-64.86	22.07	1095.01	-2.94	0.46	
bare tundra	August- September	-80.89	23.58	1095.29	-3.43	0.15	
bog	June- September	-47.75	25.24	1095.65	-1.89	0.99	
bog	July- June	67.22	22.48	1095.01	2.99	0.42	
bog	July- September	19.47	25.24	1095.65	0.77	1.00	
bog	August- June	65.04	22.48	1095.01	2.89	0.50	
bog	August- July	-2.19	22.48	1095.01	-0.10	1.00	
bog	August- September	17.29	25.24	1095.65	0.68	1.00	
deciduous forest	June- September	174.65	17.72	1095.32	9.85	0.00	***
deciduous forest	July- June	-164.36	17.35	1095.83	-9.47	0.00	***
deciduous forest	July- September	10.29	18.08	1095.25	0.57	1.00	
deciduous forest	August- June	-156.62	17.01	1096.15	-9.21	0.00	***
deciduous forest	August- July	7.74	17.35	1095.83	0.45	1.00	
deciduous forest	August- September	18.03	17.72	1095.32	1.02	1.00	
evergreen forest	June- September	70.00	17.49	1095.28	4.00	0.02	*
evergreen forest	July- June	-41.08	16.86	1095.01	-2.44	0.85	
evergreen forest	July- September	28.91	17.49	1095.28	1.65	1.00	
evergreen forest	August- June	-65.78	17.90	1096.71	-3.67	0.07	
evergreen forest	August- July	-24.70	17.90	1096.71	-1.38	1.00	
evergreen forest	August- September	4.22	18.45	1096.59	0.23	1.00	
fen	June- September	-12.46	15.67	1095.61	-0.80	1.00	
fen	July- June	73.96	14.06	1095.01	5.26	0.00	***
fen	July- September	61.49	15.67	1095.61	3.92	0.03	*
fen	August- June	97.25	14.44	1095.57	6.74	0.00	***
fen	August- July	23.29	14.44	1095.57	1.61	1.00	
fen	August- September	84.79	15.96	1095.47	5.31	0.00	***
permafrost bog	June- September	-5.25	27.80	1095.16	-0.19	1.00	
permafrost bog	July- June	35.50	23.84	1095.01	1.49	1.00	
permafrost bog	July- September	30.25	27.80	1095.16	1.09	1.00	
permafrost bog	August- June	42.93	25.93	1095.98	1.66	1.00	
permafrost bog	August- July	7.43	25.93	1095.98	0.29	1.00	
permafrost bog	August- September	37.67	29.48	1095.25	1.28	1.00	
shrub tundra	June- September	37.73	14.84	1095.29	2.54	0.78	
shrub tundra	July- June	-78.77	13.96	1095.01	-5.64	0.00	***
shrub tundra	July- September	-41.04	14.84	1095.29	-2.77	0.61	
shrub tundra	August- June	-107.63	13.96	1095.01	-7.71	0.00	***
shrub tundra	August- July	-28.86	13.96	1095.01	-2.07	0.98	
shrub tundra	August- September	-69.89	14.84	1095.29	-4.71	0.00	**
tundra wetland	June- September	32.21	23.41	1095.15	1.38	1.00	
tundra wetland	July- June	81.58	22.90	1095.01	3.56	0.10	
tundra wetland	July- September	113.79	23.41	1095.15	4.86	0.00	***
tundra wetland	August- June	14.87	22.17	1095.24	0.67	1.00	
tundra wetland	August- July	-66.71	22.17	1095.24	-3.01	0.41	
tundra wetland	August- September	47.08	22.73	1095.56	2.07	0.97	



679 *Table A6. ART-ANOVA summary table for monthly differences of N<sub>2</sub>O flux between land*  
 680 *cover types*

land cover	month	estimate	SE	df	t.ratio	p.value	sig
bare tundra	June- September	169.20	85.28	1096.41	1.98	0.99	
bare tundra	July- June	88.39	79.90	1091.13	1.11	1.00	
bare tundra	July- September	257.59	85.28	1096.41	3.02	0.40	
bare tundra	August- June	64.21	79.90	1091.13	0.80	1.00	
bare tundra	August- July	-24.18	79.90	1091.13	-0.30	1.00	
bare tundra	August- September	233.42	85.28	1096.41	2.74	0.63	
bog	June- September	269.47	91.17	1101.04	2.96	0.45	
bog	July- June	-144.95	82.19	1093.07	-1.76	1.00	
bog	July- September	124.53	91.91	1102.57	1.35	1.00	
bog	August- June	-123.70	81.37	1091.13	-1.52	1.00	
bog	August- July	21.24	82.19	1093.07	0.26	1.00	
bog	August- September	145.77	91.17	1101.04	1.60	1.00	
deciduous forest	June- September	-26.69	64.09	1096.88	-0.42	1.00	
deciduous forest	July- June	-83.51	62.96	1104.15	-1.33	1.00	
deciduous forest	July- September	-110.20	65.73	1094.72	-1.68	1.00	
deciduous forest	August- June	-40.82	61.32	1111.63	-0.67	1.00	
deciduous forest	August- July	42.69	62.96	1104.15	0.68	1.00	
deciduous forest	August- September	-67.50	64.09	1096.88	-1.05	1.00	
evergreen forest	June- September	20.48	63.24	1096.27	0.32	1.00	
evergreen forest	July- June	53.06	61.03	1091.13	0.87	1.00	
evergreen forest	July- September	73.54	63.24	1096.27	1.16	1.00	
evergreen forest	August- June	196.00	64.92	1123.01	3.02	0.40	
evergreen forest	August- July	142.94	64.92	1123.01	2.20	0.95	
evergreen forest	August- September	216.48	66.87	1117.63	3.24	0.25	
fen	June- September	61.12	57.00	1099.78	1.07	1.00	
fen	July- June	-124.04	50.90	1091.13	-2.44	0.85	
fen	July- September	-62.92	57.00	1099.78	-1.10	1.00	
fen	August- June	-141.57	52.17	1098.29	-2.71	0.65	
fen	August- July	-17.53	52.17	1098.29	-0.34	1.00	
fen	August- September	-80.45	58.07	1099.08	-1.39	1.00	
permafrost bog	June- September	144.03	100.60	1093.73	1.43	1.00	
permafrost bog	July- June	-61.83	86.31	1091.13	-0.72	1.00	
permafrost bog	July- September	82.19	100.60	1093.73	0.82	1.00	
permafrost bog	August- June	-61.84	93.55	1107.18	-0.66	1.00	
permafrost bog	August- July	-0.01	93.55	1107.18	-0.00	1.00	
permafrost bog	August- September	82.19	106.63	1095.23	0.77	1.00	
shrub tundra	June- September	122.27	54.22	1097.25	2.25	0.93	
shrub tundra	July- June	109.57	50.54	1091.13	2.17	0.95	
shrub tundra	July- September	231.85	54.22	1097.25	4.28	0.01	**
shrub tundra	August- June	-36.89	50.54	1091.13	-0.73	1.00	
shrub tundra	August- July	-146.46	50.54	1091.13	-2.90	0.50	
shrub tundra	August- September	85.39	54.22	1097.25	1.57	1.00	
tundra wetland	June- September	175.04	84.70	1094.23	2.07	0.98	
tundra wetland	July- June	-68.19	82.92	1091.13	-0.82	1.00	
tundra wetland	July- September	106.85	84.70	1094.23	1.26	1.00	
tundra wetland	August- June	-317.59	80.19	1095.48	-3.96	0.03	*
tundra wetland	August- July	-249.40	80.19	1095.48	-3.11	0.33	
tundra wetland	August- September	-142.55	82.10	1102.33	-1.74	1.00	

681

682



## 683 References

- 684 Aalto, J., Tyystjärvi, V., Niittynen, P., Kemppinen, J., Rissanen, T., Gregow, H., and Luoto, M.:  
685 Microclimate temperature variations from boreal forests to the tundra, *Agricultural and Forest*  
686 *Meteorology*, 323, 109037, <https://doi.org/10.1016/j.agrformet.2022.109037>, 2022.
- 687 Batjes, N. H.: Harmonized soil property values for broad-scale modelling (WISE30sec) with  
688 estimates of global soil carbon stocks, *Geoderma*, 269, 61–68,  
689 <https://doi.org/10.1016/j.geoderma.2016.01.034>, 2016.
- 690 Biasi, C., Rusalimova, O., Meyer, H., Kaiser, C., Wanek, W., Barsukov, P., Junger, H., and Richter, A.:  
691 Temperature-dependent shift from labile to recalcitrant carbon sources of arctic heterotrophs,  
692 *Rapid Communications in Mass Spectrometry*, 19, 1401–1408,  
693 <https://doi.org/10.1002/rcm.1911>, 2005.
- 694 Biskaborn, B. K., Smith, S. L., Noetzi, J., Matthes, H., Vieira, G., Streletskiy, D. A., Schoeneich, P.,  
695 Romanovsky, V. E., Lewkowicz, A. G., Abramov, A., Allard, M., Boike, J., Cable, W. L.,  
696 Christiansen, H. H., Delaloye, R., Diekmann, B., Drozdov, D., Etzelmüller, B., Grosse, G.,  
697 Guglielmin, M., Ingeman-Nielsen, T., Isaksen, K., Ishikawa, M., Johannsson, M., Johannsson, H.,  
698 Joo, A., Kaverin, D., Kholodov, A., Konstantinov, P., Kröger, T., Lambiel, C., Lanckman, J.-P.,  
699 Luo, D., Malkova, G., Meiklejohn, I., Moskalenko, N., Oliva, M., Phillips, M., Ramos, M., Sannel,  
700 A. B. K., Sergeev, D., Seybold, C., Skryabin, P., Vasiliev, A., Wu, Q., Yoshikawa, K., Zheleznyak,  
701 M., and Lantuit, H.: Permafrost is warming at a global scale, *Nat Commun*, 10, 264,  
702 <https://doi.org/10.1038/s41467-018-08240-4>, 2019.
- 703 Brummell, M. E., Farrell, R. E., and Siciliano, S. D.: Greenhouse gas soil production and surface  
704 fluxes at a high arctic polar oasis, *Soil Biology and Biochemistry*, 52, 1–12,  
705 <https://doi.org/10.1016/j.soilbio.2012.03.019>, 2012.
- 706 Butterbach-Bahl, K., Baggs, E. M., Dannenmann, M., Kiese, R., and Zechmeister-Boltenstern, S.:  
707 Nitrous oxide emissions from soils: how well do we understand the processes and their  
708 controls?, *Philosophical Transactions of the Royal Society B: Biological Sciences*, 368,  
709 20130122, <https://doi.org/10.1098/rstb.2013.0122>, 2013.
- 710 Cai, C., Zhang, X., Wu, M., Liu, T., Lai, C.-Y., Frank, J., He, B., Marcellin, E., Guo, J., Hu, S., and Yuan,  
711 Z.: Roles and opportunities for microbial anaerobic oxidation of methane in natural and  
712 engineered systems, *Energy & Environmental Science*, 14, 4803–4830,  
713 <https://doi.org/10.1039/D1EE00708D>, 2021.
- 714 Chapuis-Lardy, L., Wrage, N., Metay, A., Chotte, J.-L., and Bernoux, M.: Soils, a sink for N<sub>2</sub>O? A  
715 review, *Global Change Biology*, 13, 1–17, <https://doi.org/10.1111/j.1365-2486.2006.01280.x>,  
716 2007.
- 717 Cheng, C., Zhang, J., He, Q., Wu, H., Chen, Y., Xie, H., and Pavlostathis, S. G.: Exploring  
718 simultaneous nitrous oxide and methane sink in wetland sediments under anoxic conditions,  
719 *Water Research*, 194, 116958, <https://doi.org/10.1016/j.watres.2021.116958>, 2021.
- 720 Christiansen, J. R., Romero, A. J. B., Jørgensen, N. O. G., Glaring, M. A., Jørgensen, C. J., Berg, L. K.,  
721 and Elberling, B.: Methane fluxes and the functional groups of methanotrophs and  
722 methanogens in a young Arctic landscape on Disko Island, West Greenland, *Biogeochemistry*,  
723 122, 15–33, <https://doi.org/10.1007/s10533-014-0026-7>, 2015.



- 724 Clough, T. J., Rochette, P., Thomas, S. M., Pihlatie, M., Christiansen, J. R., and Thorman, R. E.: Global  
725 Research Alliance N<sub>2</sub>O chamber methodology guidelines: Design considerations, *Journal of*  
726 *Environmental Quality*, 49, 1081–1091, <https://doi.org/10.1002/jeq2.20117>, 2020.
- 727 Corbett, J. E., Tfaily, M. M., Burdige, D. J., Cooper, W. T., and Glaser, P. H.: Partitioning pathways of  
728 CO<sub>2</sub> production in peatlands with stable carbon isotopes, *Biogeochemistry*, 114, 327–340,  
729 <https://doi.org/10.1007/s10533-012-9813-1>, 2013.
- 730 Deslippe, J. R., Hartmann, M., Simard, S. W., and Mohn, W. W.: Long-term warming alters the  
731 composition of Arctic soil microbial communities, *FEMS Microbiology Ecology*, 82, 303–315,  
732 <https://doi.org/10.1111/j.1574-6941.2012.01350.x>, 2012.
- 733 Elkin, L. A., Kay, M., Higgins, J. J., and Wobbrock, J. O.: An Aligned Rank Transform Procedure for  
734 Multifactor Contrast Tests, in: *The 34th Annual ACM Symposium on User Interface Software*  
735 *and Technology*, 754–768, <https://doi.org/10.1145/3472749.3474784>, 2021.
- 736 Emmerton, C. A., St. Louis, V. L., Lehnherr, I., Humphreys, E. R., Rydz, E., and Kosolofski, H. R.: The  
737 net exchange of methane with high Arctic landscapes during the summer growing season,  
738 *Biogeosciences*, 11, 3095–3106, <https://doi.org/10.5194/bg-11-3095-2014>, 2014.
- 739 Hinrichs, K.-U. and Boetius, A.: The Anaerobic Oxidation of Methane: New Insights in Microbial  
740 Ecology and Biogeochemistry, in: *Ocean Margin Systems*, edited by: Wefer, G., Billett, D.,  
741 Hebbeln, D., Jørgensen, B. B., Schlüter, M., and van Weering, T. C. E., Springer, Berlin,  
742 Heidelberg, 457–477, [https://doi.org/10.1007/978-3-662-05127-6\\_28](https://doi.org/10.1007/978-3-662-05127-6_28), 2003.
- 743 Hugelius, G., Loisel, J., Chadburn, S., Jackson, R. B., Jones, M., MacDonald, G., Marushchak, M.,  
744 Olefeldt, D., Packalen, M., Siewert, M. B., Treat, C., Turetsky, M., Voigt, C., and Yu, Z.: Large  
745 stocks of peatland carbon and nitrogen are vulnerable to permafrost thaw, *Proceedings of the*  
746 *National Academy of Sciences*, 117, 20438–20446, <https://doi.org/10.1073/pnas.1916387117>,  
747 2020.
- 748 Hugelius, G., Ramage, J., Burke, E., Chatterjee, A., Smallman, T. L., Aalto, T., Bastos, A., Biasi, C.,  
749 Canadell, J. G., Chandra, N., Chevallier, F., Ciais, P., Chang, J., Feng, L., Jones, M. W., Kleinen,  
750 T., Kuhn, M., Lauerwald, R., Liu, J., López-Blanco, E., Luijkx, I. T., Marushchak, M. E., Natali, S.  
751 M., Niwa, Y., Olefeldt, D., Palmer, P. I., Patra, P. K., Peters, W., Potter, S., Poulter, B., Rogers, B.  
752 M., Riley, W. J., Saunois, M., Schuur, E. a. G., Thompson, R. L., Treat, C., Tsuruta, A., Turetsky,  
753 M. R., Virkkala, A.-M., Voigt, C., Watts, J., Zhu, Q., and Zheng, B.: Permafrost Region  
754 Greenhouse Gas Budgets Suggest a Weak CO<sub>2</sub> Sink and CH<sub>4</sub> and N<sub>2</sub>O Sources, But  
755 Magnitudes Differ Between Top-Down and Bottom-Up Methods, *Global Biogeochemical*  
756 *Cycles*, 38, e2023GB007969, <https://doi.org/10.1029/2023GB007969>, 2024.
- 757 Jiang, J., Yan, Z., Jian, J., Peng, S., Tian, H., Morris, K. A., Ellam, R. M., Christiansen, J. R., Chen, H.,  
758 Dong, J., Li, S.-L., Fu, P., Guan, D., Yu, G., Liu, C.-Q., Ciais, P., and Bond-Lamberty, B.: Global  
759 Soil Methane Uptake Estimated by Scaling Up Local Measurements, *Global Change Biology*, 31,  
760 e70194, <https://doi.org/10.1111/gcb.70194>, 2025.
- 761 Karjalainen, S. K., Anttila, J., Maanavilja, L., Hamedianfar, A., and Laine, A. M.: Carbon dioxide and  
762 methane gas exchange following sphagnum moss harvesting in boreal peatland, *Journal of*  
763 *Environmental Management*, 373, 123357, <https://doi.org/10.1016/j.jenvman.2024.123357>,  
764 2025.



- 765 Kemppinen, J., Niittynen, P., Rissanen, T., Tyystjärvi, V., Aalto, J., and Luoto, M.: Soil Moisture  
766 Variations From Boreal Forests to the Tundra, *Water Resources Research*, 59,  
767 e2022WR032719, <https://doi.org/10.1029/2022WR032719>, 2023.
- 768 Kits, K. D., Klotz, M. G., and Stein, L. Y.: Methane oxidation coupled to nitrate reduction under  
769 hypoxia by the Gammaproteobacterium *Methylomonas denitrificans*, sp. nov. type strain FJG1,  
770 *Environmental Microbiology*, 17, 3219–3232, <https://doi.org/10.1111/1462-2920.12772>, 2015.
- 771 Knox, S. H., Jackson, R. B., Poulter, B., McNicol, G., Fluet-Chouinard, E., Zhang, Z., Hugelius, G.,  
772 Bousquet, P., Canadell, J. G., Saunio, M., Papale, D., Chu, H., Keenan, T. F., Baldocchi, D.,  
773 Torn, M. S., Mammarella, I., Trotta, C., Aurela, M., Bohrer, G., Campbell, D. I., Cescatti, A.,  
774 Chamberlain, S., Chen, J., Chen, W., Dengel, S., Desai, A. R., Euskirchen, E., Friborg, T.,  
775 Gasbarra, D., Goded, I., Goeckede, M., Heimann, M., Helbig, M., Hirano, T., Hollinger, D. Y.,  
776 Iwata, H., Kang, M., Klatt, J., Krauss, K. W., Kutzbach, L., Lohila, A., Mitra, B., Morin, T. H.,  
777 Nilsson, M. B., Niu, S., Noormets, A., Oechel, W. C., Peichl, M., Peltola, O., Reba, M. L.,  
778 Richardson, A. D., Runkle, B. R. K., Ryu, Y., Sachs, T., Schäfer, K. V. R., Schmid, H. P., Shurpali,  
779 N., Sonnentag, O., Tang, A. C. I., Ueyama, M., Vargas, R., Vesala, T., Ward, E. J., Windham-  
780 Myers, L., Wohlfahrt, G., and Zona, D.: FLUXNET-CH<sub>4</sub> Synthesis Activity: Objectives,  
781 Observations, and Future Directions, *Bulletin of the American Meteorological Society*, 100,  
782 2607–2632, <https://doi.org/10.1175/BAMS-D-18-0268.1>, 2019.
- 783 Knox, S. H., Bansal, S., McNicol, G., Schafer, K., Sturtevant, C., Ueyama, M., Valach, A. C.,  
784 Baldocchi, D., Delwiche, K., Desai, A. R., Euskirchen, E., Liu, J., Lohila, A., Malhotra, A., Melling,  
785 L., Riley, W., Runkle, B. R. K., Turner, J., Vargas, R., Zhu, Q., Alto, T., Fluet-Chouinard, E.,  
786 Goeckede, M., Melton, J. R., Sonnentag, O., Vesala, T., Ward, E., Zhang, Z., Feron, S., Ouyang,  
787 Z., Alekseychik, P., Aurela, M., Bohrer, G., Campbell, D. I., Chen, J., Chu, H., Dalmagro, H. J.,  
788 Goodrich, J. P., Gottschalk, P., Hirano, T., Iwata, H., Jurasinski, G., Kang, M., Koebisch, F.,  
789 Mammarella, I., Nilsson, M. B., Ono, K., Peichl, M., Peltola, O., Ryu, Y., Sachs, T., Sakabe, A.,  
790 Sparks, J. P., Tuittila, E.-S., Vourlitis, G. L., Wong, G. X., Windham-Myers, L., Poulter, B., and  
791 Jackson, R. B.: Identifying dominant environmental predictors of freshwater wetland methane  
792 fluxes across diurnal to seasonal time scales, *Global Change Biology*, 27, 3582–3604,  
793 <https://doi.org/10.1111/gcb.15661>, 2021.
- 794 Kolb, S. and Horn, M. A.: Microbial CH<sub>4</sub> and N<sub>2</sub>O Consumption in Acidic Wetlands, *Front. Microbiol.*,  
795 3, <https://doi.org/10.3389/fmicb.2012.00078>, 2012.
- 796 Kopecký, M., Macek, M., and Wild, J.: Topographic Wetness Index calculation guidelines based on  
797 measured soil moisture and plant species composition, *Science of The Total Environment*, 757,  
798 143785, <https://doi.org/10.1016/j.scitotenv.2020.143785>, 2021.
- 799 Korrensalo, A., Männistö, E., Alekseychik, P., Mammarella, I., Rinne, J., Vesala, T., and Tuittila, E.-S.:  
800 Small spatial variability in methane emission measured from a wet patterned boreal bog,  
801 *Biogeosciences*, 15, 1749–1761, <https://doi.org/10.5194/bg-15-1749-2018>, 2018.
- 802 Kuhn, M. A., Varner, R. K., Bastviken, D., Crill, P., MacIntyre, S., Turetsky, M., Walter Anthony, K.,  
803 McGuire, A. D., and Olefeldt, D.: BAWLD-CH<sub>4</sub>: a comprehensive dataset of methane fluxes from  
804 boreal and arctic ecosystems, *Earth System Science Data*, 13, 5151–5189,  
805 <https://doi.org/10.5194/essd-13-5151-2021>, 2021.



- 806 Li, Z., Shang, Y., Wang, C., Wang, J., Liu, X., Li, F., Chen, G., Cheng, H., Zou, J., and Liu, S.: Generally  
807 Reduced Sink Capacity of Upland Soils for Atmospheric Methane Over the Past Three Decades  
808 (1993–2022), *Global Change Biology*, 31, e70248, <https://doi.org/10.1111/gcb.70248>, 2025.
- 809 Livingston, G. P. and Hutchinson, G. L.: of trace gas exchange: applications and sources of error,  
810 *Biogenic trace gases: measuring emissions from soil and water*, 14, 2009.
- 811 Lohila, A., Aurela, M., Hatakka, J., Pihlatie, M., Minkkinen, K., Penttilä, T., and Laurila, T.: Responses  
812 of N<sub>2</sub>O fluxes to temperature, water table and N deposition in a northern boreal fen, *European*  
813 *Journal of Soil Science*, 61, 651–661, <https://doi.org/10.1111/j.1365-2389.2010.01265.x>, 2010.
- 814 Lohila, A., Aalto, T., Aurela, M., Hatakka, J., Tuovinen, J.-P., Kilkki, J., Penttilä, T., Vuorenmaa, J.,  
815 Hänninen, P., Sutinen, R., Viisanen, Y., and Laurila, T.: Large contribution of boreal upland  
816 forest soils to a catchment-scale CH<sub>4</sub> balance in a wet year, *Geophysical Research Letters*, 43,  
817 2946–2953, <https://doi.org/10.1002/2016GL067718>, 2016.
- 818 Martins, C. S. C., Nazaries, L., Delgado-Baquerizo, M., Macdonald, C. A., Anderson, I. C., Hobbie, S.  
819 E., Venterea, R. T., Reich, P. B., and Singh, B. K.: Identifying environmental drivers of  
820 greenhouse gas emissions under warming and reduced rainfall in boreal–temperate forests,  
821 *Functional Ecology*, 31, 2356–2368, <https://doi.org/10.1111/1365-2435.12928>, 2017.
- 822 Marushchak, M. E., Pitkämäki, A., Koponen, H., Biasi, C., Seppälä, M., and Martikainen, P. J.: Hot  
823 spots for nitrous oxide emissions found in different types of permafrost peatlands, *Global*  
824 *Change Biology*, 17, 2601–2614, <https://doi.org/10.1111/j.1365-2486.2011.02442.x>, 2011.
- 825 Moore, T. R. and Dalva, M.: The influence of temperature and water table position on carbon dioxide  
826 and methane emissions from laboratory columns of peatland soils, *Journal of Soil Science*, 44,  
827 651–664, <https://doi.org/10.1111/j.1365-2389.1993.tb02330.x>, 1993.
- 828 Muhammad, L. N.: Guidelines for repeated measures statistical analysis approaches with basic  
829 science research considerations, *J Clin Invest*, 133, e171058,  
830 <https://doi.org/10.1172/JCI171058>, n.d.
- 831 Myers-Smith, I. H., Forbes, B. C., Wilkening, M., Hallinger, M., Lantz, T., Blok, D., Tape, K. D., Macias-  
832 Fauria, M., Sass-Klaassen, U., Lévesque, E., Boudreau, S., Ropars, P., Hermanutz, L., Trant, A.,  
833 Collier, L. S., Weijers, S., Rozema, J., Rayback, S. A., Schmidt, N. M., Schaepman-Strub, G.,  
834 Wipf, S., Rixen, C., Ménard, C. B., Venn, S., Goetz, S., Andreu-Hayles, L., Elmendorf, S.,  
835 Ravolainen, V., Welker, J., Grogan, P., Epstein, H. E., and Hik, D. S.: Shrub expansion in tundra  
836 ecosystems: dynamics, impacts and research priorities, *Environ. Res. Lett.*, 6, 045509,  
837 <https://doi.org/10.1088/1748-9326/6/4/045509>, 2011.
- 838 Olefeldt, D., Turetsky, M. R., Crill, P. M., and McGuire, A. D.: Environmental and physical controls on  
839 northern terrestrial methane emissions across permafrost zones, *Global Change Biology*, 19,  
840 589–603, <https://doi.org/10.1111/gcb.12071>, 2013.
- 841 Olefeldt, D., Hovemyr, M., Kuhn, M. A., Bastviken, D., Bohn, T. J., Connolly, J., Crill, P., Euskirchen, E.  
842 S., Finkelstein, S. A., Genet, H., Grosse, G., Harris, L. I., Heffernan, L., Helbig, M., Hugelius, G.,  
843 Hutchins, R., Juutinen, S., Lara, M. J., Malhotra, A., Manies, K., McGuire, A. D., Natali, S. M.,  
844 O'Donnell, J. A., Parmentier, F.-J. W., Räsänen, A., Schädel, C., Sonnentag, O., Strack, M., Tank,  
845 S. E., Treat, C., Varner, R. K., Virtanen, T., Warren, R. K., and Watts, J. D.: The Boreal–Arctic  
846 Wetland and Lake Dataset (BAWLD), *Earth System Science Data*, 13, 5127–5149,  
847 <https://doi.org/10.5194/essd-13-5127-2021>, 2021.



- 848 Patrignani, A. and Ochsner, T. E.: Canopeo: A Powerful New Tool for Measuring Fractional Green  
849 Canopy Cover, *Agronomy Journal*, 107, 2312–2320, <https://doi.org/10.2134/agronj15.0150>,  
850 2015.
- 851 Pavelka, M., Acosta, M., Kiese, R., Altimir, N., Brümmer, C., Crill, P., Darenova, E., Fuß, R., Gielen, B.,  
852 Graf, A., Klemedtsson, L., Lohila, A., Longdoz, B., Lindroth, A., Nilsson, M., Jiménez, S. M.,  
853 Merbold, L., Montagnani, L., Peichl, M., Pihlatie, M., Pumpanen, J., Ortiz, P. S., Silvennoinen, H.,  
854 Skiba, U., Vestin, P., Weslien, P., Janous, D., and Kutsch, W.: Standardisation of chamber  
855 technique for CO<sub>2</sub>, N<sub>2</sub>O and CH<sub>4</sub> fluxes measurements from terrestrial ecosystems,  
856 *International Agrophysics*, 32, 569–587, <https://doi.org/10.1515/intag-2017-0045>, 2018.
- 857 Pessi, I. S., Viitamäki, S., Virkkala, A.-M., Eronen-Rasmus, E., Delmont, T. O., Marushchak, M. E.,  
858 Luoto, M., and Hultman, J.: In-depth characterization of denitrifier communities across different  
859 soil ecosystems in the tundra, *Environmental Microbiome*, 17, 30,  
860 <https://doi.org/10.1186/s40793-022-00424-2>, 2022.
- 861 Peterson, R. A.: Finding Optimal Normalizing Transformations via bestNormalize, *The R Journal*, 13,  
862 294–313, <https://doi.org/10.32614/RJ-2021-041>, 2021.
- 863 Pihlatie, M. K., Christiansen, J. R., Aaltonen, H., Korhonen, J. F. J., Nordbo, A., Rasilo, T., Benanti, G.,  
864 Giebels, M., Helmy, M., Sheehy, J., Jones, S., Juszczak, R., Klefoth, R., Lobo-do-Vale, R., Rosa,  
865 A. P., Schreiber, P., Serça, D., Vicca, S., Wolf, B., and Pumpanen, J.: Comparison of static  
866 chambers to measure CH<sub>4</sub> emissions from soils, *Agricultural and Forest Meteorology*, 171–172,  
867 124–136, <https://doi.org/10.1016/j.agrformet.2012.11.008>, 2013.
- 868 Rantanen, M., Karpechko, A. Y., Lipponen, A., Nordling, K., Hyvärinen, O., Ruosteenoja, K., Vihma, T.,  
869 and Laaksonen, A.: The Arctic has warmed nearly four times faster than the globe since 1979,  
870 *Commun Earth Environ*, 3, 1–10, <https://doi.org/10.1038/s43247-022-00498-3>, 2022.
- 871 Rautakoski, H., Korkiakoski, M., Mäkelä, J., Koskinen, M., Minkkinen, K., Aurela, M., Ojanen, P., and  
872 Lohila, A.: Exploring temporal and spatial variation of nitrous oxide flux using several years of  
873 peatland forest automatic chamber data, *Biogeosciences*, 21, 1867–1886,  
874 <https://doi.org/10.5194/bg-21-1867-2024>, 2024.
- 875 Reeburgh, W. S.: Oceanic Methane Biogeochemistry, *Chem. Rev.*, 107, 486–513,  
876 <https://doi.org/10.1021/cr050362v>, 2007.
- 877 R: The R Project for Statistical Computing: <https://www.r-project.org/>, last access: 5 May 2026.
- 878 Repo, M. E., Susiluoto, S., Lind, S. E., Jokinen, S., Elsakov, V., Biasi, C., Virtanen, T., and Martikainen,  
879 P. J.: Large N<sub>2</sub>O emissions from cryoturbated peat soil in tundra, *Nature Geosci*, 2, 189–192,  
880 <https://doi.org/10.1038/ngeo434>, 2009.
- 881 Rinne, J., Tuittila, E.-S., Peltola, O., Li, X., Raivonen, M., Alekseychik, P., Haapanala, S., Pihlatie, M.,  
882 Aurela, M., Mammarella, I., and Vesala, T.: Temporal Variation of Ecosystem Scale Methane  
883 Emission From a Boreal Fen in Relation to Temperature, Water Table Position, and Carbon  
884 Dioxide Fluxes, *Global Biogeochemical Cycles*, 32, 1087–1106,  
885 <https://doi.org/10.1029/2017GB005747>, 2018.
- 886 Rissanen, A. J., Ojanen, P., Stenberg, L., Larmola, T., Anttila, J., Tuominen, S., Minkkinen, K.,  
887 Koskinen, M., and Mäkipää, R.: Vegetation impacts ditch methane emissions from boreal  
888 forestry-drained peatlands—Moss-free ditches have an order-of-magnitude higher emissions



- 889 than moss-covered ditches, *Front. Environ. Sci.*, 11,  
890 <https://doi.org/10.3389/fenvs.2023.1121969>, 2023.
- 891 Riutta, T., Laine, J., Aurela, M., Rinne, J., Vesala, T., Laurila, T., Haapanala, S., Pihlatie, M., and  
892 Tuittila, E.-S.: Spatial variation in plant community functions regulates carbon gas dynamics in  
893 a boreal fen ecosystem, *Tellus B: Chemical and Physical Meteorology*, 59, 838–852,  
894 <https://doi.org/10.1111/j.1600-0889.2007.00302.x>, 2007.
- 895 Saunio, M., Martinez, A., Poulter, B., Zhang, Z., Raymond, P. A., Regnier, P., Canadell, J. G., Jackson,  
896 R. B., Patra, P. K., Bousquet, P., Ciais, P., Dlugokencky, E. J., Lan, X., Allen, G. H., Bastviken, D.,  
897 Beerling, D. J., Belikov, D. A., Blake, D. R., Castaldi, S., Crippa, M., Deemer, B. R., Dennison, F.,  
898 Etiope, G., Gedney, N., Höglund-Isaksson, L., Holgerson, M. A., Hopcroft, P. O., Hugelius, G.,  
899 Ito, A., Jain, A. K., Janardan, R., Johnson, M. S., Kleinen, T., Krummel, P. B., Lauerwald, R., Li,  
900 T., Liu, X., McDonald, K. C., Melton, J. R., Mühle, J., Müller, J., Murguía-Flores, F., Niwa, Y.,  
901 Noce, S., Pan, S., Parker, R. J., Peng, C., Ramonet, M., Riley, W. J., Rocher-Ros, G., Rosentreter,  
902 J. A., Sasakawa, M., Segers, A., Smith, S. J., Stanley, E. H., Thanwerdas, J., Tian, H., Tsuruta, A.,  
903 Tubiello, F. N., Weber, T. S., van der Werf, G. R., Worthy, D. E. J., Xi, Y., Yoshida, Y., Zhang, W.,  
904 Zheng, B., Zhu, Q., Zhu, Q., and Zhuang, Q.: Global Methane Budget 2000–2020, *Earth System  
905 Science Data*, 17, 1873–1958, <https://doi.org/10.5194/essd-17-1873-2025>, 2025.
- 906 Shan, J., Sanford, R. A., Chee-Sanford, J., Ooi, S. K., Löffler, F. E., Konstantinidis, K. T., and Yang, W.  
907 H.: Beyond denitrification: The role of microbial diversity in controlling nitrous oxide reduction  
908 and soil nitrous oxide emissions, *Global Change Biology*, 27, 2669–2683,  
909 <https://doi.org/10.1111/gcb.15545>, 2021.
- 910 Simonen, Ahti (1990). *Bedrock of Finland*. In Alalammi, Pentti (ed.): *Atlas of Finland*, Part I, Sheets  
911 23–26, *Geology*, 1–4.
- 912 Smemo, K. A. and Yavitt, J. B.: Anaerobic oxidation of methane: an underappreciated aspect of  
913 methane cycling in peatland ecosystems?, *Biogeosciences*, 8, 779–793,  
914 <https://doi.org/10.5194/bg-8-779-2011>, 2011.
- 915 Stocker, T.: *Climate Change 2013: The Physical Science Basis: Working Group I Contribution to the  
916 Fifth Assessment Report of the Intergovernmental Panel on Climate Change*, Cambridge  
917 University Press, 1553 pp., 2014.
- 918 Strack, M., Waddington, J. M., and Tuittila, E.-S.: Effect of water table drawdown on northern  
919 peatland methane dynamics: Implications for climate change, *Global Biogeochemical Cycles*,  
920 18, <https://doi.org/10.1029/2003GB002209>, 2004.
- 921 Suominen, J., Li, Q., Lehtonen, A., and Mäkipää, R.: Short Term Effects of Soil Disturbance on  
922 Greenhouse Gas Fluxes on a Nutrient-Rich Peatland After Clearcutting, *Soil Use and  
923 Management*, 42, e70218, <https://doi.org/10.1111/sum.70218>, 2026.
- 924 Tan, X., Nie, W.-B., Lu, Y., Wang, X.-W., Dang, C.-C., Wang, X., Liu, L.-Y., Ren, N.-Q., Ni, B.-J., and Xie,  
925 G.-J.: Anaerobic methane oxidation drives simultaneous nitrite and nitrous oxide removal,  
926 *Bioresource Technology*, 423, 132247, <https://doi.org/10.1016/j.biortech.2025.132247>, 2025.
- 927 Throckmorton, H. M., Heikoop, J. M., Newman, B. D., Altmann, G. L., Conrad, M. S., Muss, J. D.,  
928 Perkins, G. B., Smith, L. J., Torn, M. S., Wulfschlegel, S. D., and Wilson, C. J.: Pathways and  
929 transformations of dissolved methane and dissolved inorganic carbon in Arctic tundra



- 930 watersheds: Evidence from analysis of stable isotopes, *Global Biogeochemical Cycles*, 29,  
931 1893–1910, <https://doi.org/10.1002/2014GB005044>, 2015.
- 932 Triches, N., Bolek, A., Rovamo, M., Lamprecht, R., Hashmi, W., Yazbeck, T., Ivanova, K., Eves, N.,  
933 Paul, D., Virkkala, A.-M., Vesala, T., Biasi, C., Marushchak, M., and Goeckede, M.: Between light  
934 and dark, source and sink: N<sub>2</sub>O dynamics in a subarctic, nutrient-poor permafrost peatland,  
935 <https://doi.org/10.21203/rs.3.rs-8204920/v1>, 15 December 2025 [PREPRINT].
- 936 Tupek, B., Minkinen, K., Pumpanen, J., Vesala, T., and Nikinmaa, E.: CH<sub>4</sub> and N<sub>2</sub>O dynamics in the  
937 boreal forest–mire ecotone, *Biogeosciences*, 12, 281–297, [https://doi.org/10.5194/bg-12-281-](https://doi.org/10.5194/bg-12-281-2015)  
938 [2015](https://doi.org/10.5194/bg-12-281-2015), 2015.
- 939 Turetsky, M. R., Kotowska, A., Bubier, J., Dise, N. B., Crill, P., Hornibrook, E. R. C., Minkinen, K.,  
940 Moore, T. R., Myers-Smith, I. H., Nykänen, H., Olefeldt, D., Rinne, J., Saarnio, S., Shurpali, N.,  
941 Tuittila, E.-S., Waddington, J. M., White, J. R., Wickland, K. P., and Wilkening, M.: A synthesis of  
942 methane emissions from 71 northern, temperate, and subtropical wetlands, *Global Change*  
943 *Biology*, 20, 2183–2197, <https://doi.org/10.1111/gcb.12580>, 2014.
- 944 Valenzuela, E. I., Padilla-Loma, C., Gómez-Hernández, N., López-Lozano, N. E., Casas-Flores, S.,  
945 and Cervantes, F. J.: Humic Substances Mediate Anaerobic Methane Oxidation Linked to  
946 Nitrous Oxide Reduction in Wetland Sediments, *Front. Microbiol.*, 11,  
947 <https://doi.org/10.3389/fmicb.2020.00587>, 2020.
- 948 Virkkala, A.-M., Aalto, J., Rogers, B. M., Tagesson, T., Treat, C. C., Natali, S. M., Watts, J. D., Potter, S.,  
949 Lehtonen, A., Mauritz, M., Schuur, E. A. G., Kochendorfer, J., Zona, D., Oechel, W., Kobayashi,  
950 H., Humphreys, E., Goeckede, M., Iwata, H., Lafleur, P. M., Euskirchen, E. S., Bokhorst, S.,  
951 Marushchak, M., Martikainen, P. J., Elberling, B., Voigt, C., Biasi, C., Sonnentag, O., Parmentier,  
952 F.-J. W., Ueyama, M., Celis, G., St.Louis, V. L., Emmerton, C. A., Peichl, M., Chi, J., Järveoja, J.,  
953 Nilsson, M. B., Oberbauer, S. F., Torn, M. S., Park, S.-J., Dolman, H., Mammarella, I., Chae, N.,  
954 Poyatos, R., López-Blanco, E., Christensen, T. R., Kwon, M. J., Sachs, T., Holl, D., and Luoto, M.:  
955 Statistical upscaling of ecosystem CO<sub>2</sub> fluxes across the terrestrial tundra and boreal domain:  
956 Regional patterns and uncertainties, *Global Change Biology*, 27, 4040–4059,  
957 <https://doi.org/10.1111/gcb.15659>, 2021.
- 958 Virkkala, A.-M., Niittyinen, P., Kemppinen, J., Marushchak, M. E., Voigt, C., Hensgens, G., Kerttula, J.,  
959 Happonen, K., Tyystjärvi, V., Biasi, C., Hultman, J., Rinne, J., and Luoto, M.: High-resolution  
960 spatial patterns and drivers of terrestrial ecosystem carbon dioxide, methane, and nitrous oxide  
961 fluxes in the tundra, *Biogeosciences*, 21, 335–355, <https://doi.org/10.5194/bg-21-335-2024>,  
962 2024.
- 963 Virkkala, A.-M., Wargowsky, I., Vogt, J., Kuhn, M. A., Madaan, S., O’Keefe, R., Windholz, T., Arndt, K.  
964 A., Rogers, B. M., Watts, J. D., Kent, K., Goeckede, M., Olefeldt, D., Rocher-Ros, G., Schuur, E. A.  
965 G., Bastviken, D., Aalstad, K., Aho, K., Ala-Könni, J., Alcock, H., Althuizen, I., Arp, C. D.,  
966 Asanuma, J., Attermeyer, K., Aurela, M., Balathandayuthabani, S., Barr, A., Barret, M.,  
967 Batkhisig, O., Biasi, C., Björkman, M. P., Black, A., Blanc-Betes, E., Bodmer, P., Boike, J.,  
968 Bolek, A., Bouchard, F., Bussmann, I., Cabrol, L., Canfora, E., Carey, S., Castro-Morales, K.,  
969 Chae, N., Christen, A., Christensen, T. R., Christiansen, C. T., Chu, H., Clark, G., Clayer, F.,  
970 Crill, P., Cunada, C., Davidson, S. J., Dean, J. F., Dengel, S., Detto, M., Dieleman, C., Domine,  
971 F., Dyukarev, E., Edgar, C., Elberling, B., Emmerton, C. A., Euskirchen, E., Falvo, G., Friborg, T.,  
972 Garneau, M., Giamberini, M., Glagolev, M. V., Gonzalez-Meler, M. A., Granath, G.,  
973 Guðmundsson, J., Happonen, K., Harazono, Y., Harris, L., Hashemi, J., Hasson, N., Heerah, J.,



- 974 Heffernan, L., Helbig, M., Helgason, W., Heliasz, M., Henry, G., Hensgens, G., Hiyama, T., Hock,  
975 M., Holl, D., Holmes, B., Holst, J., Holst, T., Hould-Gosselin, G., Humphreys, E., Hung, J.,  
976 Huotari, J., Ikawa, H., Ilyasov, D. V., Ishikawa, M., Iwahana, G., Iwata, H., Jackowicz-Korczynski,  
977 M. A., Jansen, J., et al.: ABCFlux v2: Arctic&ndash;boreal CO<sub>2</sub> and CH<sub>4</sub> monthly flux  
978 observations and ancillary information across terrestrial and freshwater ecosystems, Earth  
979 System Science Data Discussions, 1–86, <https://doi.org/10.5194/essd-2025-585>, 2025  
980 [PREPRINT].
- 981 Voigt, C., Marushchak, M. E., Abbott, B. W., Biasi, C., Elberling, B., Siciliano, S. D., Sonnentag, O.,  
982 Stewart, K. J., Yang, Y., and Martikainen, P. J.: Nitrous oxide emissions from permafrost-affected  
983 soils, *Nat Rev Earth Environ*, 1, 420–434, <https://doi.org/10.1038/s43017-020-0063-9>, 2020.
- 984 Voigt, C., Virkkala, A.-M., Hould Gosselin, G., Bennett, K. A., Black, T. A., Detto, M., Chevrier-Dion,  
985 C., Guggenberger, G., Hashmi, W., Kohl, L., Kou, D., Marquis, C., Marsh, P., Marushchak, M. E.,  
986 Nestic, Z., Nykänen, H., Saarela, T., Sauheitl, L., Walker, B., Weiss, N., Wilcox, E. J., and  
987 Sonnentag, O.: Arctic soil methane sink increases with drier conditions and higher ecosystem  
988 respiration, *Nat. Clim. Chang.*, 13, 1095–1104, <https://doi.org/10.1038/s41558-023-01785-3>,  
989 2023.
- 990 Whalen, S. C.: Biogeochemistry of Methane Exchange between Natural Wetlands and the  
991 Atmosphere, *Environmental Engineering Science*, 22, 73–94,  
992 <https://doi.org/10.1089/ees.2005.22.73>, 2005.
- 993 Whalen, S. C., Reeburgh, W. S., and Sandbeck, K. A.: Rapid Methane Oxidation in a Landfill Cover  
994 Soil, *Applied and Environmental Microbiology*, 56, 3405–3411,  
995 <https://doi.org/10.1128/aem.56.11.3405-3411.1990>, 1990.
- 996 Wild, J., Kopecký, M., Macek, M., Šanda, M., Jankovec, J., and Haase, T.: Climate at ecologically  
997 relevant scales: A new temperature and soil moisture logger for long-term microclimate  
998 measurement, *Agricultural and Forest Meteorology*, 268, 40–47,  
999 <https://doi.org/10.1016/j.agrformet.2018.12.018>, 2019.
- 1000 Wobbrock, J. O., Findlater, L., Gergle, D., and Higgins, J. J.: The aligned rank transform for  
1001 nonparametric factorial analyses using only anova procedures, in: *Proceedings of the SIGCHI*  
1002 *Conference on Human Factors in Computing Systems*, 143–146,  
1003 <https://doi.org/10.1145/1978942.1978963>, 2011.
- 1004 Yao, X., Wang, J., and Hu, B.: How methanotrophs respond to pH: A review of ecophysiology, *Front.*  
1005 *Microbiol.*, 13, <https://doi.org/10.3389/fmicb.2022.1034164>, 2023.
- 1006 Yeo, I. and Johnson, R. A.: A new family of power transformations to improve normality or symmetry,  
1007 *Biometrika*, 87, 954–959, <https://doi.org/10.1093/biomet/87.4.954>, 2000.
- 1008 Zhang, H., Tuittila, E.-S., Korrensalo, A., Laine, A. M., Uljas, S., Welti, N., Kerttula, J., Maljanen, M.,  
1009 Elliott, D., Vesala, T., and Lohila, A.: Methane production and oxidation potentials along a fen-  
1010 bog gradient from southern boreal to subarctic peatlands in Finland, *Global Change Biology*,  
1011 27, 4449–4464, <https://doi.org/10.1111/gcb.15740>, 2021.
- 1012